INTRAMOLECULAR VIBRATIONAL ENERGY REDISTRIBUTION IN AROMATIC MOLECULES

Andrea Callegari

A DISSERTATION
PRESENTED TO THE FACULTY
OF PRINCETON UNIVERSITY
IN CANDIDACY FOR THE DEGREE
OF DOCTOR OF PHILOSOPHY

RECOMMENDED FOR ACCEPTANCE
BY THE DEPARTMENT OF CHEMISTRY

June 1998

Abstract

Using a molecular beam optothermal spectrometer coupled via fiber optic to a 1.5 μm color center laser by a resonant build-up cavity we have measured the high resolution CH stretching first overtone spectra of three aromatic molecules—benzene (C_6H_6), pyrrole (C_4H_5N), and triazine ($C_3H_3N_3$).

In the energy region investigated ($\approx 6000\,cm^{-1}$), the calculated values for the density of coupled vibrational states for the chosen molecules are all comparable. The high resolution (6 MHz) achieved in the molecular beam environment, the high sensitivity obtained with the combined use of bolometric detection and the resonant power build-up cavity—which enhances the laser power experienced by the molecules in the beam by up to a factor 500—and the use—when necessary—of double resonance techniques have allowed us to observe the very fractionated spectra with the eigenstate resolution necessary for their subsequent assignment and analysis.

Despite their similar size, density of bath states and nature of the chromophore, the three molecules investigated show remarkably different dynamics, in terms of lifetime, number of effectively coupled states and strength of the couplings. In the case of benzene and pyrrole, statistical analysis of the energy level distribution—performed in order to test for regularity in the underlying dynamics—reveals mixed but not statistical redistribution of the initial vibrational excitation. The latter finding runs contrary to the assumptions commonly made in the statistical theories of chemical reaction rates.

Acknowledgments

I feel very fortunate that the so many people have been around during this years to make this experience truly enjoyable. It is a pleasure to acknowledge all of them for this remarkable experience, which has enriched me well beyond the achievement represented by this thesis.

I would like to start with those who have worked in the background (at least those that I know about): Ilse and Giok-Lam, your contribution to the well being of the group can not be overstated, Larry and Werner you managed to deal with my endless attempts to add a new piece to the machine, our departmental factotum John, and "monsieur" Claude and Bart at Physics, I bothered you so many times with the oddest request for some electronics, and Lou you managed to keep even my spot in lab clean.

It goes without saying that this thesis could not have been written had I not come to Princeton, for which I'm grateful to my Italian mentors Paolo, Alberto and Mauro, who introduced me to the world molecular spectroscopy, and eventually to Princeton.

It has been a pleasure to spend these years with so many friends around: the "italian connection" Alessandra, Rita, Matteo, Gianfranco, home felt closer with you around; Terri, thanks for your friendship and support; the "fun connection" (as well as co-workers) Hemant (who also taught me all the computer science that I know), Irene, Susan, André, Carlo, Peter, Marcel, Frank, Udo, Joe, it has been good to share it all with you; Paul, thanks for all the many interesting conversations and for help with the CO_2 laser. the Scoles-Lehmann group, simply the best around. A special thanks deserve those of the above who spent long nights in lab collecting data and my brother Carlo for sharing the highs and the lows of these many years.

Among those who have worked to make this happen I would like to thank the readers of this thesis, Prof. McClure, Giacinto and Kevin for the dedication and attention you have given to it, and Ilse, Carlo, Hemant, André and Scott for all the help. Thanks Martin for all the interesting discussions, and Brooks for all your constructive advice.

Giacinto and Kevin you are by far those who deserve the most credit for this work and for teaching me the concept of doing science, with a constant dedication and availability, which goes far beyond your role of advisors.

Of course none of this would have even happened without my family, your love, encouragement, understanding, support and example throughout all these years (and those before) is truly what has make all of this possible. Grazie, Mamma, Papà, Anna, Luisa, Giovanni, Carlo.

Finally thanks again all of those who believed this was possible.

Most of all, thanks Mary, for all your love.

Contents

List of Tables

List of Figures

Chapter 1

Introduction

1.1 Historical background

Intramolecular vibrational energy redistribution (IVR), i.e. the process by which vibrational energy, initially localized in a particular mode, is redistributed among all the vibrational modes of a molecule is an ubiquitous and fundamental process which has strong influence in the kinetics and final outcome of many chemical and biochemical reactions, ranging from small molecule unimolecular decomposition and isomerization to protein folding. The problem is not a new one, since it has been more than 50 years ago that the need for a detailed understanding of IVR became evident in the attempt to explain an increasingly large body of experimental data from molecular fluorescece spectra and unimolecular reaction rates.

Slater's pioneering dynamical theory of unimolecular reaction rates [1] and the statistical theories of Rice and Marcus [2, 3] and Rosenstock *et al.* [4], from which modern theories evolved [5], raised the issue of the nature and very existence of vibrational energy redistribution. In statistical theories, IVR is assumed to be rapid and complete, in contrast with Slater's theory, in which the vibrational modes are assumed to be perfectly harmonic and non interacting and the reaction to occur only when the particular superposition of these modes causes the reaction coordinate to reach the top of the reaction barrier.

Our understanding of IVR has since then been substantially refined by the success of numerous theoretical and experimental investigations. On the theoretical side, developement of more refined models and especially the rapid growth of computational methods has allowed the study of more realistic systems with less drastic approximations. On the experimental side, new tools (among which, lasers, molecular beams and double resonance techniques) have allowed overcoming the difficulties that plagued early experiments, most notably the impossibility to prepare and study a well defined initial state. It became evident that both the assumption of no randomization or total randomizations are too strong and that real life molecules will be better described by an intermediate picture, closer to one or the other extreme depending on the molecular size and structure.

Bixon and Jortner [6] have given a set of sufficient criteria for the existence of statistical IVR in isolated molecules, requiring strong, equal coupling matrix elements between the initially prepared state and all other vibrational states, where strong means larger than the average spacing of vibrational states. The requirement of equal couplings has been relaxed by Kay [7, 8] to the more likely assumption that the couplings be strong, but allowing them to be statistically independent. Similar assumptions, although applied to quite a different multi body system, lead to the famous Gaussian Orthogonal Ensemble model proposed

by Dyson [9](see chapter 3) which has worked exceedingly well in explaining the statistical properties of the energy levels of atomic nuclei and has since become the reference model in the study of ergodic dynamics.

Both Bixon-Jortner and Kay models predict that molecules of at least 5-10 atoms are required for statistical IVR to be possible, at which point the IVR rate of the initially excited state is given by the rms coupling $\langle V^2 \rangle$ and the density of states ρ via the Fermi's golden rule:

$$\Gamma = \frac{2\pi}{\hbar} \langle V^2 \rangle \rho \tag{1.1}$$

That indeed small molecules do not relax statistically, has been uneqivocally proven by Crim and coworkers [10, 11] in a beautiful series of experiments on the bimolecular reactions of vibrationally excited H_2O and HOD at energies in excess of 13000 cm^{-1}. Quite surprisingly, even relatively large molecules (> 10 atoms) have been observed to undergo non-statistical relaxation at energies as high as 6000 cm^{-1}: Kerstel *et al.* have measured the relaxation rate of the acetylenic CH stretch in a series of $(CX_3)_3YCCH$ molecules (X={H,D}, Y={C,Si}) and found it uncorrelated with the magnitude of the total density of states. Stuchebrukhov and Marcus [12], have explained this phenomenon as due to the lack of low order couplings producing bottlenecks that prevent fast relaxation of the initially excited state.

These, and many other studies (see refs. [13–16] for recent reviews), have pushed our knowledge deeper towards a more quantitative and predictive understanding of IVR in larger molecular systems and/or at higher energies above the ground state, showing that predicting IVR from first principles poses many more subtle problems than previously thought. In fact, while predicting the density of bath states ρ to a sufficiently good approximation is easily accomplished [17], even a rough estimate of the average coupling strength ($\langle V^2 \rangle$) requires accurate knowledge of the potential energy surface and extensive calculations that

account for the presence/absence of intermediate resonant states [12], large amplitude motion [18] and extreme motion states [19], which can change rather unpredictably the expected size of couplings by several orders of magnitude.

1.2 Current issues

When are the requirements for ergodic dynamics [7–9] fulfilled (if at all) in a molecule? The aforementioned successes of statistical theories (e.g. RRKM) in predicting the rates of unimolecular reactions and of Random Matrix Theory [20] (e.g. the Gaussian Orthogonal Ensemble model) in predicting the energy spectrum of several different many-body systems, would suggest that most molecules should undergo ergodic relaxation, but a clear answer to the question is yet to be been found. As pointed out by Freed [21, 22] "perhaps it is the statistical character of the initial state which is responsible for the success of the statistical theories" and "RRKM can be formulated in a mechanistic equivalent fashion by assuming that intramolecular vibrational relaxation is slow on the time scales of molecular decomposition". As for Random Matrix Theory, it is not obvious *a priori*—and it is probably not true altogether—that, in general case, a molecule is well described as a set of oscillators, all strongly coupled with each other since a molecule is not as "connected" a system as an atomic nucleus and therefore the couplings need not be as extensive. As a mater of fact, recent studies [12, 13, 23] have shown that neither the *quick* nor the *democratic* character often attributed to the relaxation process in large molecules by statistical theories are—in reality—so ubiquitous.

The ergodicity problem is, moreover, part of the more general questions: in which way and to what extent is the knowledge gained about a specific molecule, transferable to a molecule that is 'similar' to it and how can the similarity be quantified? Is it possible—given a small number of molecular parameters—to

reliably predict the IVR rate for a given molecule and a given method of excitation? Now that different theoretical models have been able (starting from semi-empirical potential energy surfaces) to successfully reproduce the experimentally observed data in molecules as large as benzene [24, 25] and $(CH_3)_3CCCH$ [12] with density of states in some cases in excess of 10^7 /cm^{-1}, it is not just a matter of mere curiosity to know to what extent the observed dynamics can be explained by mean of some "universal law" and how much of it instead depends on the fine details of the potential energy surface and of the initially prepared states.

At the two extremes we find: on one side the case of total predictability where some sort of "group rate" can be defined and transferred from one molecule to another (in analogy with the concept of group frequency in infrared spectroscopy). On the other side total unpredictability where the dynamics of every individual molecule and initial excitation has to be worked out from first principles with great expense of computational effort. Whether real molecules lie closer (and how close) to one or the other extreme is still an open question the answering of which shall not only increase our fundamental understanding of nature, but also have a sizable practical impact in such fields as laser controlled chemistry and molecular energy transfer.

1.3 This work

A very fruitful approach in the past has been the comparative study of IVR dynamics in molecules that differ from each other only by small changes in their structure. Series of molecules have been studied in this perspective [15, 26], where each element of the series differs from the others by at most a few atoms (e.g. by isotopic substitution) while the molecule keeps the same spatial/topological structure.

A sensible approach is to study a series of molecules large enough to be

considered typical (reasonably large number of degrees of freedom, and density of coupled states), but at the same time with a simple enough structure that allows for accurate modeling. Unfortunately, the most intesting molecules and excitation energies for the purpose of studying the subtle features of IVR are often the most difficult ones from the experimentalist's point of view. Frequency resolved sudies—nowadays the most commonly used technique for the investigation of vibrational dynamics—infer the vibrational dynamics from the splitting and intensity distribution of vibrational transitions and therefore require well resolved and fully assigned spectra, which clearly is rarely possible for large molecules at high energies. Specifically, the very same fractionation pattern that is the object of the study produces, as a side effect, both severe spectral congestion and "dilution" of the transition strength, with consequent loss of resolution and sensitivity. The latter two problems are exacerbated, the first, by the small rotational constants of these molecules which produces a large rotational partition function and small separation between different rotational transitions in the spectrum, the second by the small oscillator strengths of the overtone transitions used to pump the molecule to high vibrational energies. Rotational congestion can be reduced using jet cooled molecular beams—although at the high price of a strongly reduced optical density of the sample—but all the other problems are intrinsic to the IVR regime being studied and are currently the major limitation in high resolution studies of large molecules. The recent addition to our molecular beam spectrometer [27,28] of a resonant power build-up cavity that increases the laser power experienced by the molecules in the beam by up to 600 times (while at the same time achieving a resolution of 6 MHz or 2×10^{-4} cm^{-1}) has allowed us to push further the limit on molecular size, complexity and excitation energy making possible an eigenstate resolved study of the first overtone of benzene [23]. At this point, a highly desirable comparative study of aromatic molecules became evidently feasible.

Benzene (C_6H_6), pyrrole (C_4NH_5), and triazine ($C_3N_3H_3$), the aromatic molecules chosen for this purpose, satisfy all the requirements as "benchmark systems" since they have a reasonably large number of atoms (≈ 10) but a relatively rigid structure which makes them immune from the unpredictable effects of low frequency internal rotor torsional modes that plague other potentially interesting candidates. This makes it possible to calculate the most relevant couplings from semi-empirical and *ab initio* potential energy surfaces with sufficient accuracy to make these molecules "textbook models" for the study of vibrational redistribution in a system of coupled oscillators. It is not by chance that one of these molecules (benzene) has become possibly the subject of the largest number of experiments in the history of IVR as well as a benchmark system for most theoretical models. Its early dynamics has been already succesfully investigated in this way [24, 25], showing that methods and the computational power needed to treat "real life" molecules are becoming available.

For our study we have made the natural choice of keeping the the mode of the excited chromophore (CH stretch overtone) and the excitation energy as constants. In addition we have chosen to keep the density of bath states available for coupling approximately constant, at the price of having to change slightly the ring structure rather than keeping the ring structure constant (e.g. in a series of variously deuterated/substituted benzenes) which would have made the density of coupled states change over several orders of magnitude, eventually becoming prohibitively high for the substituted species with the lowest symmetry.

The main difference between the three molecules investigated here is that they have different degrees of symmetry spanning from C_{2v} (pyrrole) to C_{3h} (triazine) to D_{6h} (Benzene) which has important consequences on the localization of the vibrational eigenfunctions and therefore on the couplings between vibrational modes.

1.4 Structure of the thesis

Before the results obtained for each of the molecules investigated are presented and discussed, in turn, in chapters 4,5 and 6, the experimental apparatus used to collect the spectra is described in chapter 2. Any relevant changes made to the experimantal setup for each specific experiment are discussed in the respective chapter. The same way, chapter 3 introduces the theoretical and technical issues relevant to the analysis and discussion of the experimental results, leaving only some particular issues to be discussed along with the experimental results that they are most relevant to. The results obtained for benzene, pyrrole and triazine are presented and discussed separately in chapter 4, 5 and 6 respectively.

Bibliography

[1] N. B. Slater. *Theory of Unimolecular Reactions.* Cornell Univ. Press, Ithaca, NY, 1959.

[2] R. A. Marcus and O. K. Rice. *J. Phys. Colloid. Chem.*, 55:894–908, 1951.

[3] R. A. Marcus and O. K. Rice. Unimolecular dissociation and free radical recombination reactions. *J. Chem. Phys.*, 20:359–364, 1952.

[4] H. M. Rosenstock, M. B. Wallenstain, A. L. Wahrhaftig, and H. Eyring. *Proc. Natl. Acad. Sci. USA*, 38:667, 1952.

[5] P. J. Robinson and K. A. Holbrook. *Unimolecular Reactions.* Wiley, New York, 1972.

[6] M. Bixon and J. Jortner. Intramolecular radiationless transitions. *J. Chem. Phys.*, 48:715–726, 1968.

[7] K. G. Kay. Dynamical treatment of unimolecular decomposition reactions. The RRKM formula. *J. Chem. Phys.*, 64:2112–2132, 1976.

[8] K. G. Kay. Theory of vibrational relaxation in isolated molecules. *J. Chem. Phys.*, 61:5205–5220, 1974.

[9] Freeman J. Dyson. Statistical theory of energy levels of complex systems I. *J. Math. Phys.*, 3(1):140, Jan-Feb 1962.

[10] M. C. Hsiao A. Sinha and F. F. Crim. *J. Chem. Phys.*, 92:6333, 1990.

[11] J. D. Themke A. Sinha and F. F. Crim. *J. Chem. Phys.*, 96:372, 1992.

[12] A. A. Stuchebrukhov and R. A. Marcus. Theoretical study of intramolecular vibrational relaxation of acetylenic CH vibration for $v = 1$ and 2 in large polyatomic molecules $(CX_3)_3YCCH$, where X=H or D and Y=C or Si. *J. Chem. Phys.*, 98(9):6004, 1993.

[13] Martin Gruebele and Robert Bigwood. Molecular vibration energy flow: beyond the golden rule. *Int. Rev. Phys. Chem*, Submitted.

[14] David J. Nesbitt and Robert W. Field. Vibrational energy flow in highly excited molecules: role of intramolecular vibrational redistribution. *J. Phys. Chem.*, 1996.

[15] K. K. Lehmann and G. Scoles. Intramolecular dynamics from eigenstate-resolved spectra. *Annu. Rev. Phys. Chem.*, 45:241–274, 1994.

[16] T. Uzer. Theories of intramolecular energy transfer. *Phys. Reports*, 199:73–146, 1991.

[17] Daniele Romanini and Kevin K. Lehmann. Numerical Laplace transform density of states calculation, for medium and large molecules, in the harmonic and first-order anharmonic approximations. *J. Chem. Phys.*, 98:6437–6444, 1993.

[18] G. A. Bethardy, X. Wang, and D. S. Perry. The role of molecular flexibility in accelerating intramolecular vibrational relaxation. *Can. J. Chem.*, 72:652–659, 1994.

[19] J. E. Gambogi, J. T. Timmermans, K. K. Lehmann, and G. Scoles. *J. Chem. Phys.*, 99:9314–9317, 1993.

[20] T. Guhr, A. Müller-Groeling, and H. A. Weidenmüller. Random matrix theories in quantum phyisics: common concepts. *Phys. Reports*, Submitted.

[21] K. F. Freed and A. Nitzan. Intramolecular vibrational energy redistribution and the time evolution of molecular fluorescence. *J. Chem. Phys.*, 73:4765–4778, 1980.

[22] K. Freed. Remarks. *Faraday Discuss. Chem. Soc.*, 67:231–235, 1979.

[23] A. Callegari, H. K. Srivastava, U. Merker, K. K. Lehmann, G. Scoles, and M. Davis. Eigenstate resolved infrared-infrared double-resonance study of intramolecular vibrational relaxation in benzene: first overtone of the CH stretch. *J. Chem. Phys*, 106:432–435, 1997.

[24] Christophe Iung and Robert E. Wyatt. Time-dependent quantum mechanical study of intramolecular vibrational energy redistribution in benzene. *J. Chem. Phys.*, 99(3):2261–2264, August 1993.

[25] Edwin L. Sibert III, William P. Reinhardt, and James T. Hynes. Intramolecular vibrational relaxation and spectra of CH and CD overtones in benzene and perdeuterobenzene. *J. Chem. Phys.*, 81(3):1115–1134, 1984.

[26] J. W. Dolce. *Intramolecular vibrational energy redistribution in ethane analogues: a high resolution infrared spectroscopy study.* PhD thesis, Princeton University, 1996.

[27] Chris J. O'Brien. Improvement to an infrared laser-molecular beam spectrometer for IVR studies. Senior Thesis, Princeton University, 1994.

[28] J. E. Gambogi, M. Becucci, C. J. O'Brien, K. K. Lehmann, and G. Scoles. Reinvestigation of the $2\nu_1$ band in trifluoropropyne using a frequency stabilized 1.5 μm color center laser in conjunction with a laser field build-up cavity. *Ber. Bunsenges. Phys. Chem.*, 99(3):548–554, 1995.

Chapter 2

Experimental

2.1 Introduction

Our approach for the study of IVR in these medium-large molecules is that of eigenstate-resolved overtone spectroscopy. Given the high density of coupled states expected ($\approx 100/\text{cm}^{-1}$), eigenstate resolution of the spectrum requires a doppler-free, collision-free environment to reduce the linewidth, and rotational/vibrational cooling of the sample to reduce the spectral congestion, all of which can be achieved by operating in a molecular beam environment [1,2]. The high resolution and sensitivity of the spectrometer used to collect the spectra presented in the next chapters are due to three key elements:

- a supersonic jet for the production of a cold, collimated molecular beam
- a resonant power build-up cavity for efficient coupling of laser radiation to the molecules in the beam
- a low temperature bolometer to detect the power deposited by the laser into the vibrational modes of the molecules in the beam.

The original version of the spectrometer along with some of the main modifications that lead to the current setup has been been described before [3–5]. Here we will briefly outline the general layout of the apparatus, describing in more detail a few key features and improvements which have been essential for carrying out the experiments reported below.

A picture of the spectrometer is shown in fig. 2.1. Schematically, it can be divided into three main parts according to their function:

- a molecular beam apparatus where a molecular beam of the species to be investigated is formed, probed and detected
- various sources of radiation used to probe the beam (microwave synthesizer, lasers, power build-up cavity etc.)
- the computer and electronics used for monitoring and controlling the system and for collecting the data.

2.2 The molecular beam apparatus

The molecular beam machine is formed by two vacuum chambers, each pumped by a 5000 l/s, oil diffusion pump. A single rotary-roots mechanical pumps combination is sufficient to back the diffusion pumps under normal operating conditions. In the first chamber, a beam of the molecule of interest is formed by expanding a diluted mixture (usually 0.5-2%) of it in helium through a 50μm diameter nozzle (Structure Probe Inc. electron microscope aperture) into a vacuum chamber at a typical stagnation pressure of 400 kPa. Upon collimation by a 0.5 mm diameter skimmer placed 12 mm downstream from the nozzle, the beam enters the second vacuum chamber where it is probed and detected. Overtone pumping of the beam is carried out with a tunable infrared laser inside a high finesse resonant cavity which dramatically increases the circulating

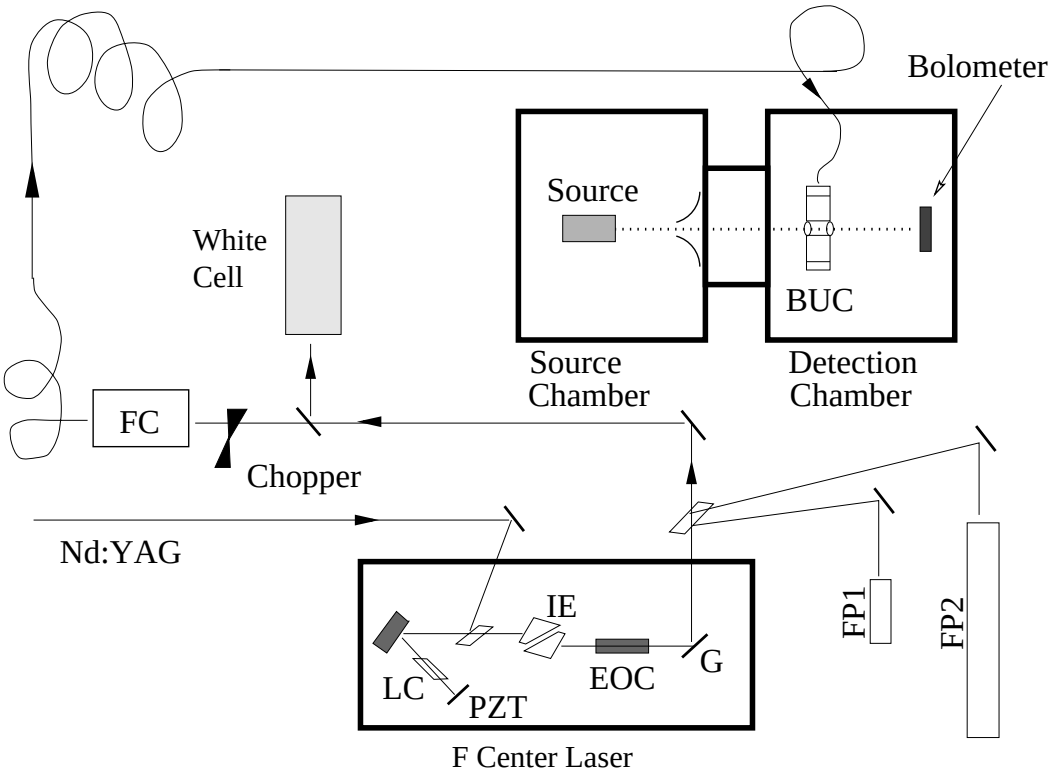

Figure 2.1: Schematic of the the molecular beam spectrometer. The following acronyms are used: PZT piezoelectric tuned mirror, LC laser crystal, IE internal etalon, EOC electro-optic crystal, G grating, FC fiber coupler, BUC build up cavity.

power experienced by the molecules (see below). Provision is made for additional sources of radiation to be coupled onto the molecular beam for double resonance experiments, in order to facilitate (or even making at all possible) the assignment of the spectra and/or to probe otherwise difficult to reach vibrational levels. Because of the long spontaneous emission lifetimes in the infrared ($\approx$ 10 ms), the increased energy gained from the beam upon excitation of a molecular vibrational transition can be efficiently detected further downstream by means of a cryogenically cooled bolometer located on the beam path. The bolometer, fabricated by Infrared Laboratories (Tucson, AZ), is of a composite silicon type, optimized for a working temperature of 1.5 K. The bolometer is enclosed in a small copper box for radiation shielding and is attached to the bottom of a liquid helium cryostat. The whole assembly is enclosed inside a second metal shield kept at the temperature of liquid nitrogen. The molecular beam reaches the bolometer through a 1.5×4 mm aperture on the second shield and a 1.5×3 mm aperture on the first shield. The two apertures are located at a distance of about 65 mm and 5 mm from the bolometer respectively. The skimmer/build-up cavity and skimmer/bolometer distance are 10 cm and 44 cm respectively. The low working temperature, achieved by pumping on the helium cryostat down to a pressure of 20 Torr, not only improves the performances of the bolometer, but also decreases the microphonic noise since helium, below the λ point (2.7 K) evaporates from the surface of the liquid instead of bubbling out of the bulk in the usual boiling process. Response of the bolometer is flat at low frequencies, with the limiting the upper operating frequency at about 400 Hz, where the 3 dB point occurs.

2.3 The radiation sources

The main source of radiation used in this work is a commercial Burleigh FCL-120 color-center laser. Laser action is provided by optical transitions of F_{2^+H} defects in a NaCl:OH crystal host pumped with 1.064 μm radiation from a Nd:YAG laser (Quantronix model 416). An auxiliary source of visible radiation (Omnichrome model 532 Argon-ion laser operated on all lines) is required to pump the crystal and reorient the optical dipole of the F-center. Both lasers are operated in a CW mode. The main pump power is limited to a maximum of 4 W in order to avoid possible damage to the crystal, whereas the auxiliary laser operating power is set to a value high enough (10 mW) that any further increase doesn't produce an appreciable increase of the color-center laser output power. Coarse tuning throughout the entire tuning range is achieved with a grating mounted in the Littrow configuration that also serves as the output coupling element. Since the laser cavity is of the "standing wave" type, one additional mode (the so called "hole burning" mode) can co-exist with the main laser mode without competing for energy, causing the laser to emit on two distinct frequencies. A low finesse intracavity etalon serves the double purpose of eliminating the "hole burning" mode and selecting one particular cavity mode for the laser to operate on, among those allowed by the broad tuning curve of the grating. Finally fine tuning of the frequency of the laser emission is achieved by controlling the cavity length through the piezo mounted cavity end-mirror. With this scheme, single mode narrowband CW tunable radiation is produced with power in excess of 250 mW in the 1.72-1.49 μm (5800-6700 cm^{-1}) wavelength region with a peak of 380 mW at 1.60 μm (6250 cm^{-1}), as shown in figure 2.2. The free running linewidth of the laser is about 15 MHz determined primarily by fluctuations of the pump Nd:YAG laser power.

The laser is tuned in 1 MHz increments at a rate of about 20 MHz/second

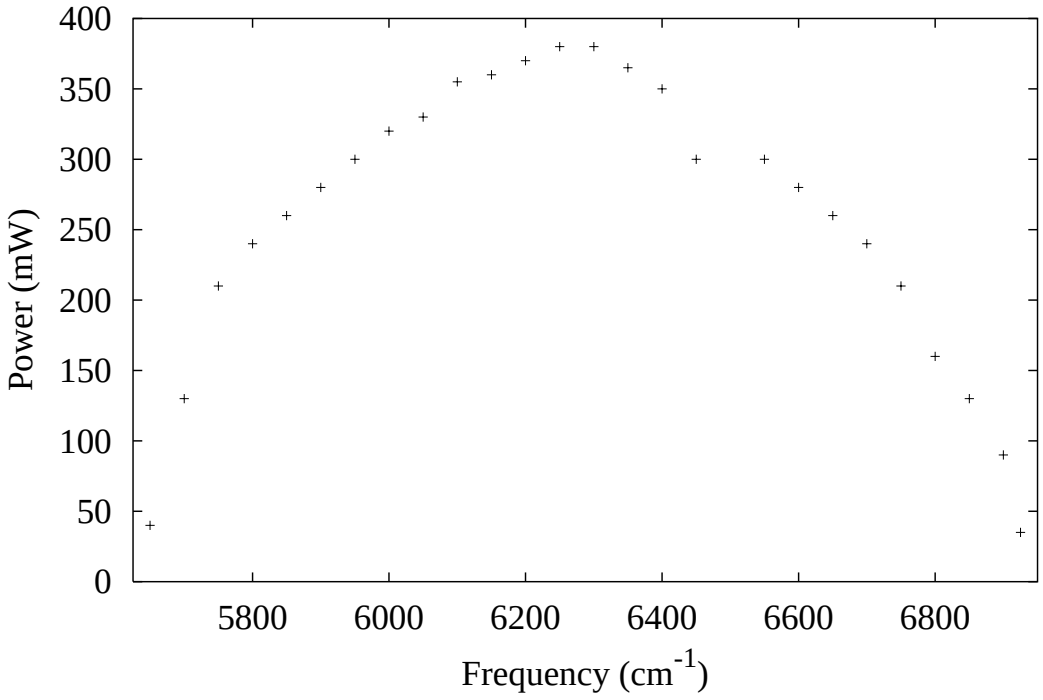

Figure 2.2: Tuning curve of the color center laser

through synchronous feed-forward of the three tuning elements. The wavelength of the emitted radiation is monitored with a wavemeter and two scanning confocal etalons of 150 and 8000 MHz free spectral range, respectively. The voltage ramp used to scan the etalons is monitored and the voltage at which a transmission maximum occurs is recorded with a sample-and-hold type circuit. The 150 MHz etalon is hermetically sealed and temperature stabilized to ± 0.01 °C to minimize frequency drifts and serves as a frequency reference. In addition, absolute calibration is achieved by simultaneously collecting the spectrum of an appropriate reference gas [6], in a White-type gas cell at a pressure of about 1 Torr. Monitoring the frequency of the laser with a scanning reference etalon

instead of using a fixed etalon as frequency marker replaces the requirement of making the laser scanning linear between two etalon marks with the much easier task of ensuring that the etalon scan is linear. As this can be readily achieved with high accuracy and moderate effort, the accuracy of the spectrometer is practically limited only by the finite resolution and the residual temperature drift of the etalon, which in turn can be made to exceed the high resolution (5 MHz) of the spectrometer. Absolute and relative accuracy of the spectrometer are typically 5 MHz and 1 MHz respectively. Single mode scanning of the laser frequency is computer controlled by forward-feeding the tuning elements (grating, internal etalon and piezo-mounted cavity mirror). Calibration of the feed-forward rate of the grating and etalon is performed before starting a scan in order to ensure that they accurately track the scanning of the cavity mode. The bolometer signal, the etalons signals and the White cell signal are converted with a 12-bit A/D board and simultaneously recorded, thus providing a one-to-one correspondence between laser frequency and bolometer signal from which the spectrum is successively extracted. The voltage ramp applied to the piezo tuning elements is reset every 500 MHz (two cavity free spectral ranges) for the cavity mirror and 21 GHz (one free spectral range) for the internal etalon. The data collected is therefore in the form of a collection of short, continuous, partially overlapping portions of the spectrum, which are subsequently joined together by partially interactive software routines to give the final version of the spectrum.

Double resonance techniques, where an additional source of radiation is used to label a particular rotational state of the molecules under investigation, has been used to facilitate (sometime make at all possible) the assignment of the very congested spectra observed. The details of the technique and the changes made to the spectrometer to implement the double resonance scheme in each specific case are discussed in the corresponding chapters.

2.4 Build-up cavity

Since the sensitivity of the spectrometer is limited by the intrinsic bolometer noise, its advantageous whenever possible to increase the circulating laser power, which directly translates into a linear increase of the number of excited molecules that reach the bolometer.[1] Quite often though, increasing the output power of the laser is not possible or economically convenient. Given a certain laser power a frequently used technique involves using a multipass cell. Gains of up to 50 fold can be achieved at the price of slightly worse resolution (when the crossings are not perpendicular to the beam), and of an increased difficulty in aligning the laser with the molecular beam.

To enhance the effective laser power experienced by the molecules in the beam we have taken a different approach based on a resonant power build-up cavity (BUC) located across the molecular beam, developed in our laboratory [4, 5]. The cavity is a high finesse etalon derived from the modified core of a Newport model SR-170-C "supercavity" optical spectrum analyzer: two curved high reflectivity ($R > 99.94\%$) low loss (< 100 ppm) dielectric mirrors are glued at the two ends of a 25 mm long piezoelectric tube thus forming a stable and compact resonator with a 6000 MHz free spectral range and a manufacturer specified finesse in excess of 5000 within 10% of the wavelength (1.55 μm) that the cavity is optimized for. Since the cavity cannot be sealed, as in the original manufacturers design, the performance is partially degraded by the presence of small amounts of contaminants on the mirrors. The experimentally measured maximum finesse is only about 3000 which corresponds to an increase of the losses to about 800 ppm. (see fig 2.3). Two 3 mm diameter holes custom drilled in the middle of the piezoelectric tube allow the molecular beam to cross

[1] This is true only far from saturation, which is the case when signal is weak because of the small transition dipole. If instead the signal is weak because the initial state has a small population, the right correcting approach is changing, if possible, the beam temperature.

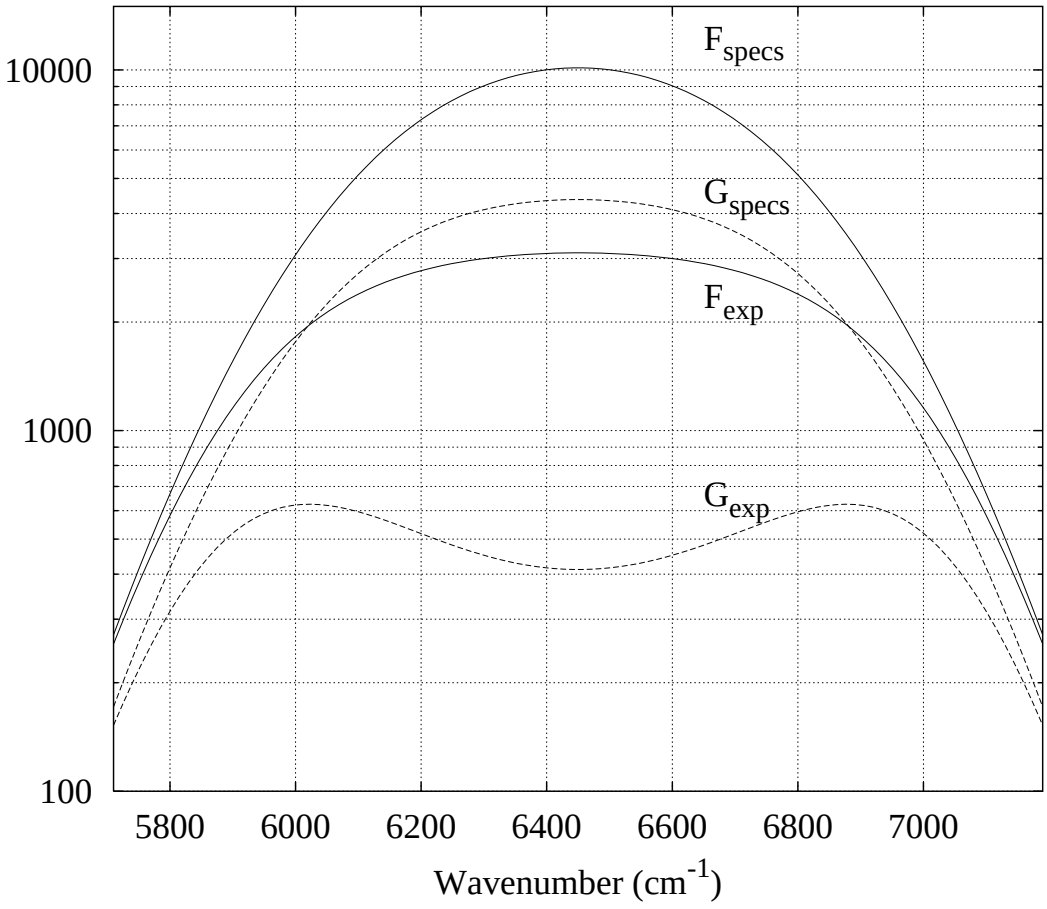

Figure 2.3: Finesse and gain factor for the build-up cavity. F_{spec} is the finesse specified by the manufacturer, G_{spec} is the corresponding circulating power gain calculated assuming 100 ppm losses. F_{exp} and G_{exp} are the same quantities calculated assuming 800 ppm losses

the BUC perpendicular to its optical axis, therefore interacting with the laser radiation inside the cavity, where the effective power is enhanced by a factor up to 600 (greater than 100 over the whole range of the laser emission frequency). The radius of curvature of the two mirrors is 30 cm, which makes the cavity non-confocal and—as a consequence—its modes non-degenerate. This achieves the maximum finesse allowed by the mirror high reflectivity and low losses, at the price of requiring accurate mode matching for optimum power coupling into the cavity. For ease and stability of the alignment, the laser is brought into the molecular beam apparatus via a single mode optical fiber and coupled to the BUC by a gradient index lens which ensures effective mode matching. About 1/3 of the original laser power is delivered through the fiber and is coupled into the cavity. The loss of power and the additional complications introduced by the optical fiber are fully compensated for by the high stability of the setup once it has been properly alligned.

The second requirement for optimum power coupling is that at all time the laser frequency coincides with one of the resonant frequencies of the build-up cavity to within a small fraction of the width (≈ 1.2 MHz) of the resonance.

Fast control of the laser frequency becomes necessary and is achieved by means of a Li:NbO_3 electro-optic crystal placed inside the laser cavity. The voltage applied across the electro-optic crystal changes its index of refraction which in turn determines the effective cavity length, and therefore the laser frequency. A sine wave voltage of frequency $f_m = 70$ KHz is applied to the crystal to modulate the instantaneous laser frequency (ν) by a small amount ($\Delta\nu \approx 50$ kHz) about its average value (ν_0):

$$\nu = \nu_0 + \Delta\nu \sin(2\pi f_m t) \tag{2.1}$$

this causes the power transmitted through the cavity ($I_t(\nu)$) to be modulated at the same frequency. In particular for a modulation depth smaller than the

transmission peak width:

$$I_t(\nu) \approx I_t(\nu_0) + \frac{\partial I(\nu_0)}{\partial \nu_0} \Delta\nu \sin(2\pi\nu_m t) \tag{2.2}$$

The transmitted power is measured with a photodiode and the modulated signal is synchronously detected with a lock-in amplifier. The derivative error signal thus obtained is amplified and fed back to the electro-optic crystal to counteract any jitter of the laser frequency away from the cavity transmission peak. Using this method the frequency jitter of the laser is now reduced to about 100 kHz. Still, since the feedback loop has a finite gain at zero frequency, large drift of the laser frequency away from the cavity transmission peak can't be corrected. For this purpose the residual error signal is integrated and fed back to the BUC to ensure proper tracking of large drifts. In practical terms the electro-optic crystal ensures compensation for the fast jitter of the laser frequency but not for slow changes of the laser frequency which is the BUC task to follow. Although it does not improve the long term stability of the laser, this "mixed feedback" scheme has been adopted since it did not require changes to the pre-existing scanning program of the laser.

The need to keep the laser and BUC locked to each other at all times contrasts with the need of chopping the laser for lock-in detection of the bolometer signal. This problem has been solved by using a partially transparent chopper whose blades block only 90 % of the laser power. In this way—at the expense of a 10 % reduction of the signal—an error signal is always available for feedback control. For optimal performance of the feedback loop the signal from the BUC photodiode is normalized to the laser power modulation with an analog multiplier (AD734), ensuring the same input level into the lock-in amplifier and the same gain of the feedback loop regardless of the chopping process.

2.5 Performance

The laser is normally chopped at about 280 Hz where the bolometer noise is lowest. The latter has a typical value of 40 nV/$\sqrt{\text{Hz}}$, close to the manufacturers specifications of 25 nV/$\sqrt{\text{Hz}}$. With the responsivity of the detector at 7.7 V/W this translates into about 5×10^{-14} W/$\sqrt{\text{Hz}}$, or a minimum detectable level of about 10^6 vibrationally excited molecules (CH overtone) per second hitting the bolometer. Since a flux of 2×10^{10} molecules per second across the laser beam is typically produced, saturating an unfractionated transition (e.g. acetylene) gives the spectrometer a dynamic range of 10000:1. The laser power available is more than 20 times larger than required to saturate one such transition, which means that even transitions that are fractionated into 10-20 components can be observed without loss of sensitivity. The highly collimated nature of the beam and the single laser crossing allowed by the build up cavity scheme reduce Doppler broadening significantly, with correspondingly great enhancement of resolution: an instrumental linewidth of about 2×10^{-4} cm^{-1} (6 MHz) is achieved, limited primarily by transit time broadening and residual Doppler broadening, which are estimated [4] to be 2.6 MHz and 2.7 MHz, respectively.

The high output power of the laser in the C-H stretching overtone region, its narrow bandwith, the availability of a power build-up cavity and the possibility of initial state selection via double resonance, make our spectrometer a uniquely ideal machine to study the vibrational relaxation of relatively large molecules at energies comparable to those tipically involved in chemical reactions, where substantial fractionation of the spectrum is expected. In particular the full potential of the apparatus is exploited in the investigation presented in this work, where the combination of high density of coupled vibrational states ($\approx 100/\text{cm}^{-1}$), small rotational constants ($B \approx 0.2 - 0.3\text{cm}^{-1}$) and extensive fractionation (10-100 states per multiplet), produces highly congested spectra with up to 1000 observed transitions per cm^{-1}.

Bibliography

[1] G. Scoles, editor. *Atomic and molecular beam methods*, volume 1. Oxford University Press, 1988.

[2] G. Scoles, editor. *Atomic and molecular beam methods*, volume 2. Oxford University Press, 1988.

[3] Erik R. Th. Kerstel, Kevin K. Lehmann, Thomas F Mentel, Brooks H. Pate, and Giacinto Scoles. Dependence of intramolecular vibrational relaxation on central atom substitution: ν_1 and $2\nu_1$ molecular beam optothermal spectra of $(CH_3)_3CCCH$ and $(CH_3)_3SiCCH$. *J. Phys. Chem.*, 95:8282, 1991.

[4] Chris J. O'Brien. Improvement to an infrared laser-molecular beam spectrometer for IVR studies. Senior Thesis, Princeton University, 1994.

[5] J. E. Gambogi, M. Becucci, C. J. O'Brien, K. K. Lehmann, and G. Scoles. Reinvestigation of the $2\nu_1$ band in trifluoropropyne using a frequency stabilized 1.5 μm color center laser in conjunction with a laser field build-up cavity. *Ber. Bunsenges. Phys. Chem.*, 99(3):548–554, 1995.

[6] Guy Guelachvili and K. Narahari Rao. *Handbook of infrared standards II.* Academic Press, Boston, 1993.

Chapter 3

Models and Data analysis

A generally used model [1] in molecular spectroscopy assumes that the molecular hamiltonian can be decomposed as:

$$H = H_0 + W \tag{3.1}$$

where H_0 is a separable hamiltonian in some set of general coordinates and W is non separable but is small enough that it can be treated with perturbation theory. In the case when W couples only a small number of states (often referred to as *sparse* IVR regime), direct deperturbation is possible and is the traditionally preferred method since it gives the most detailed informations about the perturbing states (energy, rotational constants, coupling strength). The molecules studied here fall instead in the *intermediate* to *dense* IVR regime, where the density of bath states is large compared to the average coupling strength. The number of coupled states (N) becomes too large for an exact approach to work and more statistical methods must be used.

3.1 General methods

Extracting the full $(N+1)^2$ matrix elements of W cannot be done with the sole information contained in the observed spectrum. Instead, a prediagonalized bath of dark states is assumed and the Lawrance-Knight deconvolution method [2,3] is used to extract from the observed spectrum the positions of the dark states and their couplings to the bright state. However, the information about the bath-bath couplings as well as about the rotational constants of the individual bath states is lost. This is not a severe drawback since determination of the identity of the bath states would anyways be close to impossible. Since a change of basis is a unitary transformation an important piece of information that is instead preserved is the sum of the squares of the couplings, whose J dependence (or lack of it) allows to separate contributions from anharmonic and Coriolis coupling.

Along the same line, the need to extract useful information from spectra that could not be modeled "exactly" has lead to the developement of more statistical methods of analysis where a few average quantities computed from the observed spectrum are taken as representatives of its most important features. Again, while some amount of information is thrown away in the process, the parameters that are extracted usually have an immediate physical meaning which makes them most usefull e.g. for comparison between different molecules.

When the number of states coupled to the bright state becomes large and trace of their exact identity is lost it makes more sense, rather than counting the total number of coupled states, to speak of a density of states per unit energy (or equivalently frequency). For the purpose of our discussion, the density of states available for coupling to the bright state (ρ_{calc}) is calculated from the vibrational frequencies in a harmonic normal mode approximation, using a numerical method [4] that involves inverse Laplace transform of the partition function. The total density of states thus calculated is then divided by an appropriate factor [5] which takes into account that only states that belong to the same symmetry class as the bright state can couple to it. Experimentally, the actual density of states effectively coupled to the bright state (ρ_{obs}) is determined simply as the ratio between the number of observed coupled states (N) and the energy interval that they occupy:

$$\rho_{\mathrm{obs}} = \frac{N-1}{\Delta E} \tag{3.2}$$

with the understanding that in case of poor signal to noise the number obtained can be a (sometimes severe) underestimate of the actual value.

Comparison between the observed (ρ_{obs}) vs. calculated (ρ_{calc}) density of coupled states gives some insight into the details of the couplings: severe discrepancies may suggest the presence of bottlenecks in the relaxation ($\rho_{\mathrm{obs}} \ll \rho_{\mathrm{calc}}$) or breakdown of the K symmetry ($\rho_{\mathrm{obs}} \gg \rho_{\mathrm{calc}}$) by Coriolis coupling.

Perhaps the single most important statistical parameter that can be extracted from the spectrum is the lifetime (τ) of the bright state (as discussed below). The information that is lost in this case is where the energy relaxes, which is not a severe limitation since the identity of the bath states usually cannot be determined from the observed spectra alone anyways.

There are several ways to extract the lifetime from the spectrum ($I(\omega)$), the most obvious ones related to the survival probability obtained [6] from the Fourier transform of the spectrum autocorrelation function:

$$P(t) = |\langle \Psi(t)|\Psi(0)\rangle|^2 = \int e^{-i\omega t} d\omega \int I(\omega) I(\omega - \omega') d\omega' \tag{3.3}$$

which can then be fitted with an exponential decay to determine the lifetime. Alternatively, the time when the survival probability falls below $1/e$ also can be used as an estimate of the lifetime. With a less obvious but equally valid procedure the rms coupling ($\langle V^2 \rangle$) determined with the Lawrance-Knight deconvolution procedure and the density of observed coupled states given by equation 3.2 can be substituted into the Fermi's gloden rule formula:

$$\Gamma = \frac{2\pi}{\hbar} \langle V^2 \rangle \rho \tag{3.4}$$

to give a reliable estimate [7] of the IVR rate (Γ) which is related to the lifetime of the bright state by the simple relationship:

$$\tau = \frac{1}{2\pi\Gamma}. \tag{3.5}$$

In principle either method is equally as good and in fact, they both converge to the correct number as the spectrum better approximates a true lorentzian lineshape. In practice the result obtained from a fit of the survival probability depends on a somewhat arbitrary decision about which portion of the initial decay has to be included in the fit. In contrast, extracting the lifetime with the Fermi's golden rule, although lacking the self evidence of the other methods,

yelds a unique result for a given observed spectrum, independent of the experimentalist's preference. This makes it a more objective method, especially in the case of scarcely fractionated spectra where the survival probability exhibits large recurrencies and/or oscillatory behaviour.

3.2 Random matrix theory and level spacing statistics

Ever since proposed by Wigner [8] to describe the statistical properties of nuclear energy levels, random matrix theory (RMT) [9] has been an extremely useful tool for the study of strongly coupled multi-body systems when the complexity of the problem or the approximate knowledege of the couplings make it impossible to use more exact methods. The concepts used and the assumption made in RMT are similar to those of statistical mechanics, with the difference that in the latter a statistical description of the system is needed because of ignorance about its initial state, and the statistical properties are determined by an ensemble average over all possible initial condition, while in RMT the statistical description is needed because of ignorance about the interaction itself, and the statistical properties are determined by the ensemble average over all possible Hamiltonians that could describe the system. The Gaussian Orthogonal Ensemble introduced by Dyson [10], formalized for the first time the concept of "maximum ignorance" about the Hamiltonian with the requirement that the ensemble of matrices used to describe the system be invariant under unitary transformations, and has since then been used as a reference model for all random matrix theories.

The connection of GOE with chaos discovered later [11] is of particular relevance to the so far unaswered question of whether or not intramolecular vibra-

tional energy redistribution is ergodic and which parameters control the onset of ergodicity. The atoms of a molecule, are not as confined as the particles which form the many-body systems that are well described by RMT (e.g. protons and neutrons in atomic nuclei). They are, therefore, coupled less extensively with each other, which may result in non-ergodic dynamics.

The most evident spectral signature of GOE behaviour is considered to be the occurence of energy level repulsion and spectral rigidity (long range order), corresponding to the multiple avoided crossings expected in the limit of strong couplings. A widely used probe of the occurence of energy level repulsion is the probability distribution of the normalized spacing (s) between adjacent levels [12]:

$$P(s) = as^{\beta}\exp(-bs^{\beta+1}),\ a = (\beta+1)b,\ b = \left\{\Gamma\left(\frac{\beta+2}{\beta+1}\right)\right\}^{\beta+1} \tag{3.6}$$

where the parametes β ranges between the values of 0 for a totally uncorrelated spectrum (Poisson distribution) and 1 for a GOE-like spectrum. The spectral rigidity is usually determined from the fluctuations of the staircase function $N(E)$ from a straight line $A+BE$ (where $N(E)$ is the number of levels observed with energy less then E). A good estimator for the degree of rigidity of a portion of length L of the spectrum centered at E is [13]:

$$\Delta_3(L) = \min_{A,B}\left\{\frac{1}{L}\int_{E-L/2}^{E+L/2}[N(E) - A - BE]^2 dE\right\} \tag{3.7}$$

As can be seen from fig 3.1, the L dependence of Δ_3 is markedly different for uncorrelated (Poisson) and GOE spectra, which allows to discriminate between the two cases.

Obtaining meaningful and reliabile results from both the Δ_3 and level spacing statistics depends critically on the quality of the spectra, which must be sorted into pure (same set of quantum numbers) and complete (no missing levels) sequencies. The level statistics of badly corrupted spectra—whether because several weak transitions have not been detected or spurious levels have

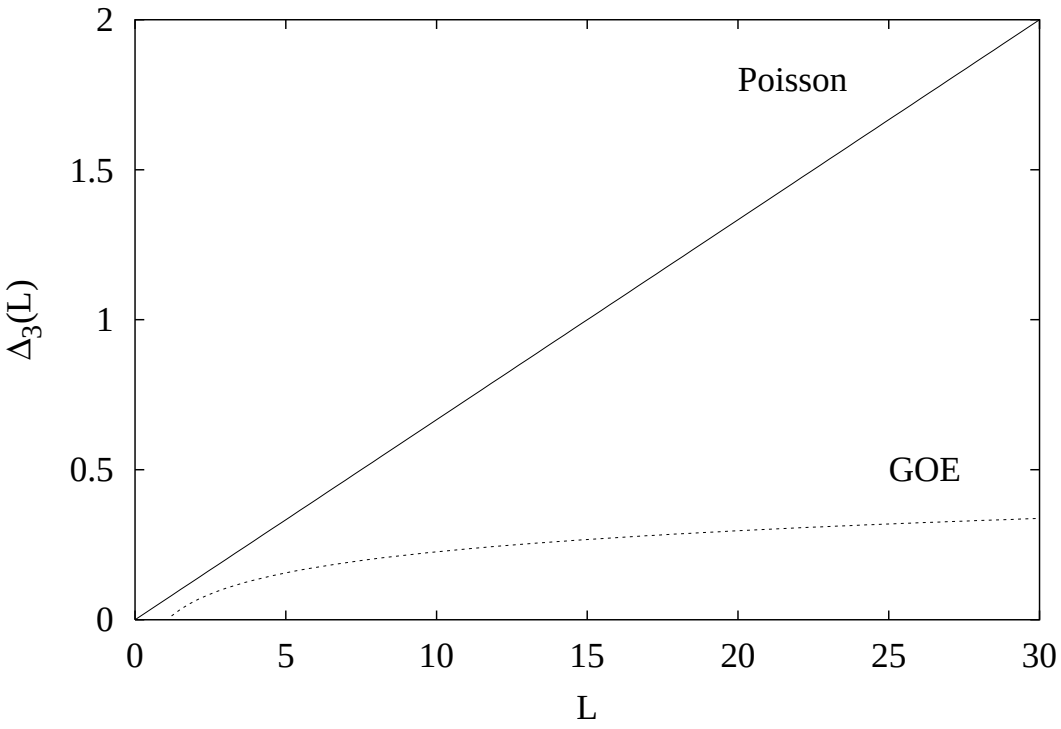

Figure 3.1: The L dependence of the Δ_3 statistics for an uncorrelated (Poisson) and GOE spectra. The value of L is normalized to the average level spacing.

been assigned to the wrong sequence—are known to resemble those of totally uncorrelated spectra, which might obviously lead to erroneous conclusions.

Lehmann and Coy [14] have devised techniques to account for missing and spurious levels, which make possible to perform statistical analysis of "imperfect" spectra, provided that a significant fraction of the transitions is observed. The details are discussed in section 4.3.1, along with the statistical analysis of the observed benzene spectrum.

Bibliography

[1] T. Uzer. Theories of intramolecular energy transfer. *Phys. Reports*, 199:73–146, 1991.

[2] W.D. Lawrence and A.E. Knight. *J. Chem. Phys.*, 89:917, 1985.

[3] K. K. Lehmann. *J. Chem. Phys.*, 95:7556, 1991.

[4] Daniele Romanini and Kevin K. Lehmann. Numerical Laplace transform density of states calculation, for medium and large molecules, in the harmonic and first-order anharmonic approximations. *J. Chem. Phys.*, 98:6437–6444, 1993.

[5] M. Quack. On the density and number of rovibronic states of a given symmetry species: rigid and nonrigid molecules, transition states and scattering channels. *J. Chem. Phys.*, 82:3277–3283, 1985.

[6] E.J. Heller. *Faraday Discuss. Chem. Soc.*, 75:141, 1983.

[7] K. G. Kay. Theory of vibrational relaxation in isolated molecules. *J. Chem. Phys.*, 61:5205–5220, 1974.

[8] E. P. Wigner. *Ann. Math.*, 53:36, 1951.

[9] T. Guhr, A. Müller-Groeling, and H. A. Weidenmüller. Random matrix theories in quantum phyisics: common concepts. *Phys. Reports*, Submitted.

[10] Freeman J. Dyson. Statistical theory of energy levels of complex systems I. *J. Math. Phys.*, 3(1):140, Jan-Feb 1962.

[11] O. Bohigas and M.-J. Giannoni. *Lecture notes in physics*, volume 209. Springer, Berlin, 1984.

[12] T. A. Brody, J. Flores, J. B. French, P. A. Mello, A. Pandey, and S. S. M. Wong. Random matrix physics: spectrum and strength fluctuations. *Rev. Mod. Phys.*, 53:385–475, 1981.

[13] Freeman J. Dyson and Madan Lal Metha. Statistical theory of energy levels of complex systems IV. *J. Math. Phys.*, 4(5):701, May 1963.

[14] K. K. Lehmann and S. L. Coy. The gaussian orthogonal ensemble with missing and spurious levels: a model for experimantal level-spacing distributions. *J. Chem. Phys.*, 87:5415–5418, 1987.

Chapter 4

The CH overtone spectrum of Benzene

4.1 Introduction

Since the pioneering work of M. Berry and coworkers [1], benzene overtones have been one of the most important model systems for study of Intramolecular Vibrational Relaxation (IVR), and have been the subject of numerous experimental and theoretical investigations [1–9]. The early experimental work [1] investigated the fundamental and overtone bands up to $v = 9$, but because of extensive inhomogeneous contributions to the spectral structure, the interpretation of these spectra remained ambiguous. Theoretical modeling by Sibert *et al.* [2] indicated that the overall spectral width of the visible bands reflects rapid IVR, via Fermi resonance between the C-H stretching local modes and the C-H bend normal modes. However, dynamics on a time scale longer than ~ 100 fs could not be inferred from the spectrum due to the rotational and hot band congestion present in these room temperature experiments.

More recent experimental work on the overtone spectrum has focused on free jet cooling of the molecules, which dramatically reduces inhomogeneous effects. Because of the lowering of the transition dipole with increasing overtone order, these experiments are restricted to the near IR, particularly the first and second overtone bands near 6000 and 8900 cm^{-1} respectively [3–5]. These experiments were carried out with pulsed laser sources of modest spectral resolution which, combined with the remaining inhomogeneous rotational structure in the the beam, lead to an effective resolution of a few cm^{-1}, limiting the study of IVR dynamics on a time scale shorter than about 1 ps.

In particular, the spectrum of the first overtone region, reported by Page *et al.* [4, 5], shows the presence of at least 30 vibrational bands, spread over a range of 300 cm^{-1} (lower panel of fig. 4.1). The bright state of this transition is believed to consist of a CH stretching excitation intermediate between local and normal mode motion [10]. The spectral structure mentioned above, arises from the mixing of this state with a manifold of states that arise from the in-plane vibrational modes. Each peak in the spectrum represents a resonance that is produced by the early time dynamics of the C-H stretch vibrational relaxation. We will refer to these states as "first order" states, to emphasize that they come from the diagonalization of the zeroth order hamiltonian perturbed with the strongest couplings. The survival probability calculated from this spectrum, reveals an IVR 'lifetime' of the bright state of 100 fs. The qualitative features of this and other experimental spectra have been reproduced in theoretical models by Iung and Wyatt [6], Zhang and Marcus [7], Iachello and Oss [8].

The next question that comes to mind is: after the initially excited state has undergone the first step of relaxation, how long will it take for full relaxation to occur? or equivalently: if one of the "first order" states is prepared as the initial state, how long is it going to survive? In order to answer these questions a higher resolution experiment was needed to break the 1 ps barrier of the

previous experiments.

The improvement of the spectrometer with the power build-up cavity described in chapter 2 has enabled us to obtain an eigenstate resolved spectrum of the first overtone band of benzene [9], thus extending the time interval over which IVR has be studied in this molecule by a factor greater than 10,000. The congestion of the spectrum deriving from the concurrent presence of extensive fractionation of the bright state, highly degenerate rotational structure and small rotational constants has been overcome by using near-IR/mid-IR double resonance to obtain the spectrum originating from a single, assigned lower rotational level of the ground vibrational state. Therefore, having eliminated the inhomogeneous rotational structure, we have been able to unambiguously prove that it takes about 20 ps for the second step of relaxation to occur and we have also obtained some evidence that full relaxation may not be achieved even at the radiative lifetime.

4.2 Experimental

The experimental setup is the same as described in chapter 2. Briefly a 1% mixture of benzene in helium is expanded in a vacuum chamber through a 50 μm nozzle at a backing pressure of 400 kPa. A 0.5 mm skimmer lets only the center portion of the free jet expansion into a second vacuum chamber, thus forming a well collimated molecular beam. Further downstream the beam is then probed by a color center laser tuned on the CH overtone region. The interaction region is located inside a resonant power build-up cavity (BUC) orthogonal to the beam that enhances the circulating power by a factor 500 in this wavelength region. Excitation of a molecular vibration is detected by a a cryogenically cooled bolometer on which the beam eventually impinges, by sensing the increased energy of the beam.

The only significant change made to the spectrometer for this particular ex-

periment has been to implement a double resonance scheme in order to isolate the contribution from a single initial rotational state out of an extremely congested spectrum: a few cm downstream from the skimmer and upstream from the BUC, the beam is pumped with about 1 W of $^{13}CO_2$ laser radiation at 9.6 μm in a single – almost orthogonal – crossing. 1 W is enough IR power to strongly saturate the ν_{14} $^rQ_0(2)$ transition which is only 17 MHz from the center of the R_{30} line of the $^{13}CO_2$ laser [11], giving about 10 μV of signal when the laser is chopped at 280 Hz.

In a single resonance spectrum an absorption signal is seen as an increase in the energy of the beam any time the color center laser hits a molecular transition. In contrast, in a double resonance experiment an absorption signal is seen (on top of the 10 μm baseline generated by the CO_2 laser) only when the transitions pumped by the two lasers share a common level. More specifically the signal appears as a dip in the baseline when the transition pumped by the second laser originates from the *lower* state of the transition pumped by the first, i.e. from a ground state molecule (V-type double resonance). Alternatively the signal appears as a peak on top of the baseline if the transition pumped by the second laser originates from the *upper* state of the transition pumped by the first i.e. from a vibrationally excited molecule (ladder type double resonance). Transitions of this second type (although not the main scope of this investigation) have been observed in the frequency region investigated here, shifted with respect to their V-type counterparts by the cross-anharmonicity of the C-H stretching with ν_{14}.

Excess noise due to power and frequency fluctuations of the laser is present in the baseline of the double resonance spectra, which brings the total measured noise to about 100 nV/$\sqrt{Hz}$. A special problem is posed by the fact that—even if the average CO_2 laser frequency is locked to the peak of the bolometer absorption signal—occasionally large frequency excursions occur, putting the laser off resonance with the molecular transition. This causes the baseline to shift down for a short moment, which could be mistaken for a double resonance signal. This highly non-gaussian character of the noise makes it difficult to distinguish signal from noise, although the observed line-shape can be used to eliminate most such noise fluctuations. In order to ensure that none of these false features were mistaken for real transitions, two scans of the same spectrum were collected under the same experimental conditions retaining only those features which appeared in both spectra.

The signal to noise ratio obtained was sufficient for the investigation of the spectrum of the strongest "first order" state (6005 cm^{-1} in the spectrum of Page *et al.*), but it was clear that eliminating the excess noise was needed to investigate the second most strong state (6000 cm^{-1}) and perform a meaningful comparison between the two spectra.

The power and frequency instabilitiy of the CO_2 laser that produces the excess noise on the baseline signal is mainly the consequence of instabilities of the discharge in the laser tube. In our case the problem was found to be caused by the imperfect insulation of one of the metal plates supporting the laser tube ZnSe windows. The metal plate occasionally acted as a second cathode diverting the plasma discharge from its normal path, thus disturbing the laser action. Once discovered, the problem was fixed by painting the metal support with with insulating laquer, which stopped the unwanted discharge. This has allowed collecting the spectrum of the second state (about half the intensity) with the same signal to noise. In this way it is possible for us to compare the dynamics of two different first order states of the overtone manifold and study its dependence on the amount of CH stretching character of the bright state.

4.3 Results and Discussion

In the bottom panel of fig. 4.1 the CH stretch overtone spectrum of benzene has been reconstructed from the data of Page *et al.* [4] as a sum of lorentzian peaks. The intensity and center position of the peaks have been taken from table I of ref. [4], and the full width at half maximum has been set to the value of 4 cm^{-1} reported there. The results of our high resolution investigation of the two strongest peaks is shown in the two top panels (note the 100 fold magnification of the frequency scale). We will refer to them as band A (6005 cm^{-1}) and B (6000 cm^{-1}) respectively.

Each of the two spectra is composed of more than 200 lines which must be

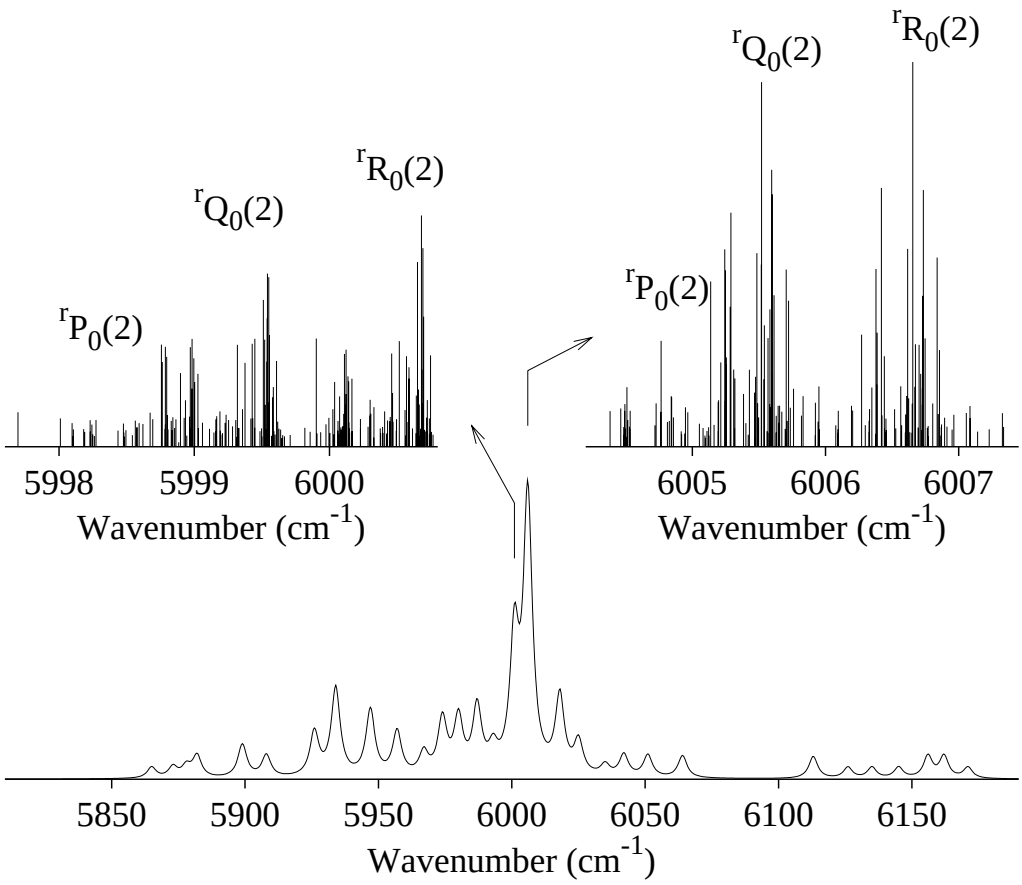

Figure 4.1: The $v = 2$ overtone spectrum of CH stretch in benzene. The spectrum in the bottom panel has been reconstructed from the data of Page *et al.* [4]; the top panels are the transitions observed in this work originating from the $J = 2, K = 0$ ground state.

assigned to a complete set of quantum numbers before proceding with analysis of the underliying dynamics. Since these are double resonance spectra, all observed transitions must originate from the $J = 2,\ K = 0$ ground state labelled by the CO_2 laser. This, in conjuction with the selection rules $\Delta J = 0, \pm 1$ and $\Delta K = \pm 1$ for a perpendicular band, restricts the candidates for an assignment to three transitions only: ${}^rR_0(2)$, ${}^rQ_0(2)$ and ${}^rP_0(2)$ corresponding to the upper rotational states $J'_{K'} = 3_1, 2_1, 1_1$ respectively. Lines corresponding to the three possible transitions are visible in the spectra as three partially overlapping clumps: ${}^rR_0(2)$ and ${}^rQ_0(2)$ with about the same relative intensity and ${}^rP_0(2)$ with about 1/3 relative intensity due to the Hönl-London factor. Since there's no ambiguity in the notation we will often refer to these clumps just as R, Q and P respectively. Because of the lower relative intensity of the P branch, several of its weaker transitions have probably disappeared into the noise, and in fact only about 60% of the lines observed in the Q or R branches do have a counterpart in the P branch, therefore P has not been used for quantitative analysis (unless otherwise specified). A preliminary assignment of each observed line to J'=1,2 or 3 has been made simply by visual inspection of the relative intensities and line positions. The assignment has been checked and—in the regions where two clumps overlap—refined by direct comparison between P,Q and R branches as shown in fig. 4.2 for the R and Q branches.

The procedure is in principle rigorously justified when transitions to the same final state are compared or when the IVR and rotational dynamics are completely separable i.e. the interaction between vibrations and rotations is negligible in comparison to the interaction between the vibrations themselves. Although the final J is not the same here, the similarities observed between different rotational levels (see fig. 4.2) point to the fact that—at least for the low J states studied here—the relaxation dynamics is strongly dominated by anharmonic coupling with negligible contribution from Coriolis coupling. It is

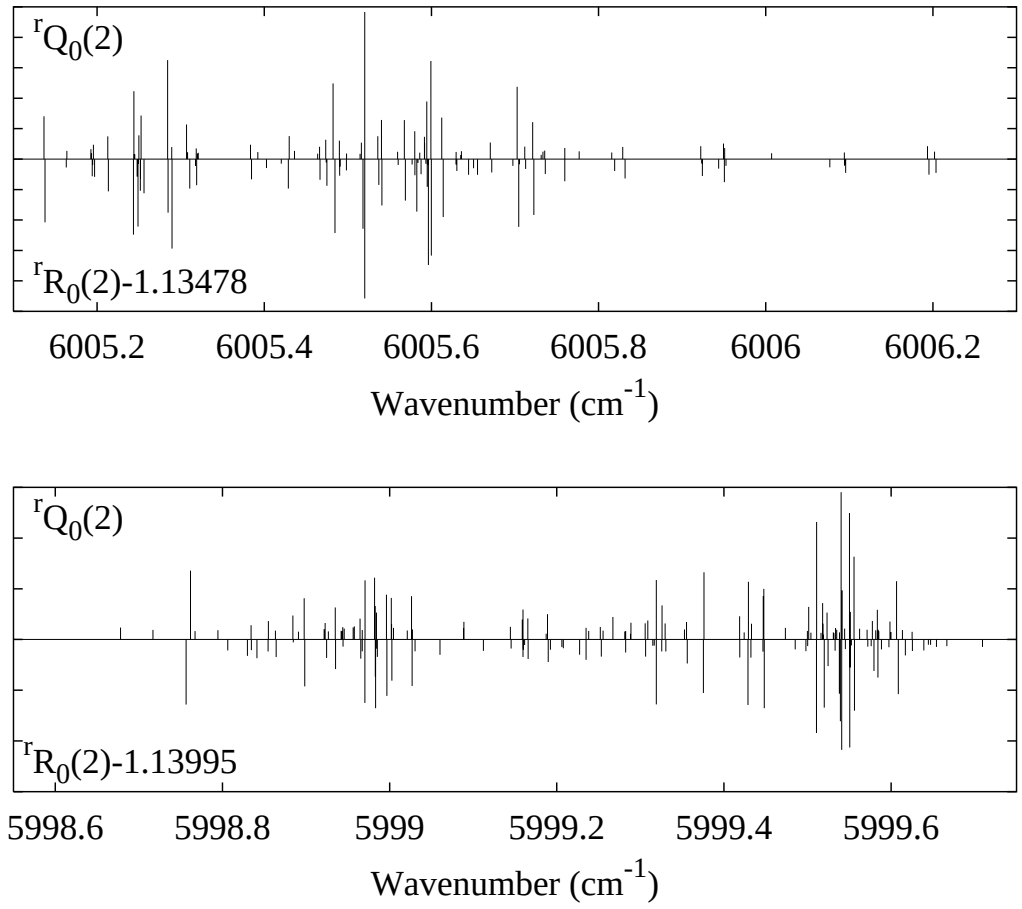

Figure 4.2: Comparison between the different transitions originating from the same $(J = 2, K = 0)$ lower state observed in the eigenstate resolved spectrum. The R branch lines (downward) are made to approximately coincide with the corresponding ones in the Q branch by shifting them down by 1.13478 and 1.13995 cm^{-1} respectively.

also quite clear from the comparison that the position of the bath states is not much different at $J = 3$ than at $J = 2$ which in turn implies that the bath states have similar rotational constants. The degree of similarity is an important parameter since it is related to the ergodicity (or lack thereof) of the dynamics, as discussed below. It can be quantified by calculating the standard deviation $\sigma_{2,3}$ of the frequency difference between pairs of corresponding lines in ${}^rQ_0(2)$ and ${}^rR_0(2)$. We assume that the bath states in the energy region under investigation have rotational constants $B' = B'' + \Delta B$ where B' is the ground state rotational constant and ΔB is normally distributed with variance σ_B. Then:

$$\sigma_{2,3} = \sqrt{\langle (\Delta B)^2 [J(J+1)_{J=3} - J(J+1)_{J=2}]^2 \rangle} = 6\sqrt{\langle (\Delta B)^2 \rangle} = 6\sigma_B \quad (4.1)$$

Unfortunately the procedure is to some extent arbitrary since it is not necessary that all the lines in one branch have a clear counterpart in the other, and in fact some of them actually don't have one. To simply disregard these lines is likely to give an underestimate of the actual value of $\sigma_{2,3}$ while just pairing them with the closest available match is likely to give an overestimate. A reasonable compromise, often used in statistical data analyis, is to calculate $\sigma_{2,3}$ with the latter procedure, discard the pairs whose mismatch is larger than 3 $\sigma_{2,3}$ and then recalculate $\sigma_{2,3}$.

The value $\sigma_B = 5 \times 10^{-4}$ cm^{-1} thus obtained can be compared with the σ_B of the bath states in the C-H stretch fundamental region, in order to quantify the different degree of mixing between the bath states at different energies. If, in fact, the bath states have the same degree of mixing in the fundamental as in the overtone region then the value of σ_B for the overtone should be twice the value for the fundamental. In fact for a state with $v_1, v_2 \ldots v_n$ quanta in mode $1, 2 \ldots n$ [12, pag. 400]:

$$\Delta B = -\sum \alpha_i v_i \quad (4.2)$$

and states in the overtone energy region have on average twice as many vibrational quanta as those in the fundamental. If, conversely mixing of the bath states increases going from the fundamental to the overtone, then their rotational constants are equalized by the mixing and the increase of σ_B is smaller than the twofold value expected. Remarkably, the value $\sigma_B = 2.1 \times 10^{-4}$ estimated for the fundamental from the 20 perturbing states observed by Pliva and Pine [13] speaks, quite unexpectedly, in favor of non-increasd mixing.

Once the lines in the spectrum have been sorted out according to their J, K quantum numbers, it's possible to start analyzing the underlying dynamics. Most of the following analysis (in particular the level spacing statistics) would be severely biased if the finite signal-to-noise would cause too many of the weakest transitions to disappear into the noise, preventing their observation. Therefore the first property that we want to analyze and compare to the expected value is the observed density of coupled states. The expected density of coupled states has been calculated from the inverse Laplace transform of the partition function [14] in the harmonic approximation with the fundamental frequencies reported by Goodmann *et al.* [15] (see table 4.1). The harmonic approximation clearly underestimates the actual density of states. However, for the low average number of quanta in each mode typical of the energy region investigated, it has been estimated [16] that the error is less than 10%.

Sym	Wilson no.	Herzberg no.	Freq. (cm^{-1})
a_{1g}	ν_2	ν_1	3073.942
	ν_1	ν_2	993.071
a_{2g}	ν_3	ν_3	1350
b_{1u}	ν_{13}	ν_5	3057
	ν_{12}	ν_6	1010
b_{2u}	ν_{14}	ν_9	1309.4
	ν_{15}	ν_{10}	1149.7
e_{2g}	ν_7	ν_{15}	3056.7
	ν_8	ν_{16}	1600.9764
	ν_9	ν_{17}	1177.776
	ν_6	ν_{18}	608.13
e_{1u}	ν_{20}	ν_{12}	3064.3674
	ν_{19}	ν_{13}	1483.9854
	ν_{18}	ν_{14}	1038.2670
a_{2u}	ν_{11}	ν_4	673.97465
b_{2g}	ν_5	ν_7	990
	ν_4	ν_8	707
e_{1g}	ν_{10}	ν_{11}	847.1
e_{2u}	ν_{17}	ν_{19}	967
	ν_{16}	ν_{20}	398

Table 4.1: Observed gas-phase fundamental frequencies of benzene, from ref. [15]

Of the calculated 1600 states/cm^{-1} at the energy of 6000 cm^{-1}, on average about 1/12 (133/cm^{-1}) have the right e_{1u} symmetry to couple to the bright state [17].

The observed density of coupled states $(N-1)/\Delta E$ is in all cases lower than

expected, but at least for the Q and R branches the observed value is at most within a factor 2 of the expected value (see table 4.3), making us confident that we do see a large fraction of the coupled states. This is especially true if we consider only the center portions of the clumps where the intensity is higher and less lines are likely to be lost into the noise. Also analysis of the spacing statistics carried out in the next section give values of the average density of states in accordance with those calculated here. The comparison between observed and calculated density of coupled states also provides insight into the nature of the couplings: for both A and B bands ρ_{obs} doesn't depend appreciably on J which confirms the initial impression that Coriolis coupling does not play a significant role in the dynamics, at least for the low-J states investigated.

The first and probably most obvious question that we want to answer is: what would be the lifetime of the first order bright state if we were to prepare it at $t = 0$ say with a short laser pulse? To estimate the IVR rate Γ, we have chosen the Fermi golden rule ($\Gamma = 2\pi\langle V^2\rangle\rho$ with the value of ρ given by $(N-1)/\Delta E$ and that of $\langle V\rangle$ by the result of Lawrance-Knight deconvolution, since, as explained in chapter 3, it gives a robust estimate of the actual rate. The values obtained are reported in table 4.3.

In all cases the lifetimes range from 10 to 20 ps, which is almost one order of magnitude longer than the estimate given by Page *et al.* [4, 5], based on the linewidth of the peaks in their spectrum, clearly limited by the finite laser resolution. Quite remarkably the observed lifetimes are comparable to the lower limit ($\tau > 21$ ps) determined by Nicholson and Lawrance [18] for the ring modes $n\nu_1$ (Wilson numbering, $n = 0 \rightarrow 7$) up to 8200 cm^{-1}. This agreement is consistent with a two steps relaxation process of the C-H stretching overtone, where in the first (fast) step the initial excitation is redistributed among the in plane modes [7] in about 100 fs, giving rise to the spectrum observed by Page *et al.*, while in the second (slow) step further redistribution occurs into

J'	E_b	N_d	$\langle V_{\rm rms}\rangle$	$\sum V_i^2$	ρ	$\rho_{\rm app}$	$\tau_{\rm GR}$
	$\rm cm^{-1}$		10^{-2} $\rm cm^{-1}$	$(10^{-2}$ $\rm cm^{-1})^2$	states/$\rm cm^{-1}$		ps
1	5998.54434	32	5.18	858	30		10
2	5999.32159	79	2.89	659	88	85(10)	11
3	6000.42639	98	2.72	725	104	105(12)	11
1	6004.72700	36	3.53	448	49		14
2	6005.50787	71	2.63	491	67	70	18
3	6006.63914	62	2.65	435	59	59	20

Table 4.2: Average properties of the IVR multiplets observed in the CH stretching overtone spectrum of benzene. The multiplets are labeled with the rotational quantum number J and energy of their parent bright state E_b: average coupling ($\langle V\rangle$) and total square of the coupling ($\sum V_i$) to the bath, number (N_d) and density ρ of observed coupled states, lifetime from Fermi's golden rule ($\tau_{\rm GR}$). The density of states calculated with the statistical methods of section 4.3.1 is also listed for comparison

the full bath of available states (which includes the out of plane modes), in 10-20 ps, thus producing the linewidth observed by Nicholson and Lawrance and the fractionation observed in this work.

The survival probability, calculated from the Fourier transformation of the spectral autocorrelation functions (fig. 4.3), yields qualitative agreement for the lifetimes (20-25 ps), when a negative exponential is fitted to the initial decay rates, although the exact value changes by a few ps, depending on which portion of the initial decay is used for the fit.

More importantly, a careful inspection of the survival probability reveals that two other important time-scales are involved in the relaxation process: the time for the first recurrence to occur and the time for damping the recurrencies. The first (95 ps for band A and 55 ps for band B) is related to the sub-structure visible in fig. 4.2, and specifically to the presence of two distinct sub-clumps in each J, K multiplet. This is the time that it takes for the excitation to oscillate back and forth between the two groups of states and it is proportional to the inverse of their separation. The second one is approximately the time that it would take for each of the sub-clumps to relax separately and can be thought of as the time for "irreversible" decay to occur.

Interestingly the damping of the recurrences seems to follow a "power law" decay (rather than an exponential one), which has been suggested [19–21] to be due to the local nature of energy flow or, in other words, on the fact that the coupling between any two states ($|\mathbf{v}'\rangle$ and $|\mathbf{v}\rangle$) decreases exponentially with the number of bonds separating the atoms involved in the vibrational motions of $|\mathbf{v}'\rangle$ and $|\mathbf{v}\rangle$ as well as with the "distance" in quantum space ($n = |\mathbf{v} - \mathbf{v}'| = \sum |\mathrm{v_i} - \mathrm{v'_i}|$) between $|\mathbf{v}'\rangle$ and $|\mathbf{v}\rangle$.

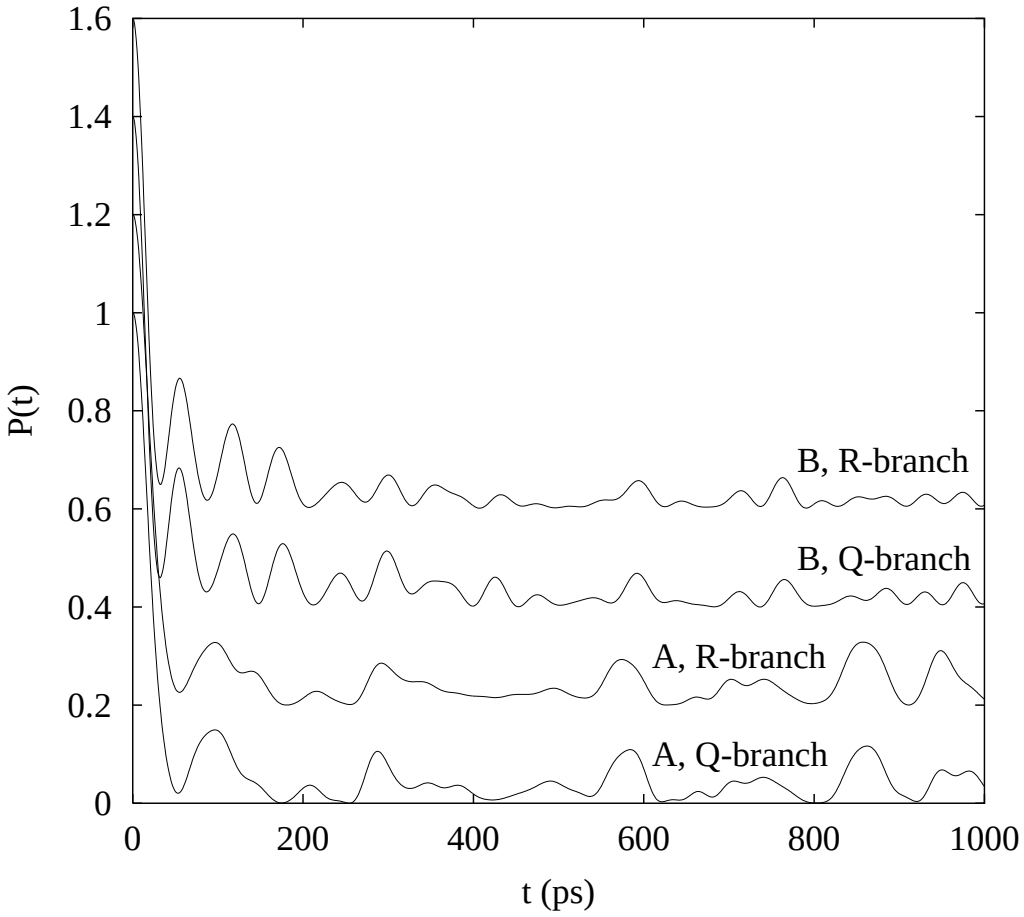

Figure 4.3: Survival probability calculated from the Fourier transform of the spectrum autocorrelation function. The band termed "A" is the one observed around 6005.5 cm^{-1}, the band termed B is the one observed around 5999.3 cm^{-1}. For greater clarity the plots are offset vertically by 0.2 from each other.

4.3.1 Level spacing statistics

The presence of sub-structure in the observed spectra implies the existence of approximately good quantum numbers corresponding to symmetries that are preserved in the early times of relaxation. One very important question is whether any approximately good quantum numbers are still preserved on the time-scale explored by the experiment (given by the resolution of the spectrometer: $\Delta t \approx 1/(2\pi\Delta\nu) \approx 25$ ns), which classically corresponds to incomplete randomization of the vibrational energy into the bath of symmetry-allowed dark states, as opposed to the complete randomization expected for chaotic dynamics. In the case where no good quantum numbers but energy and angular momentum are left, all states interact with each other and repulsion of the energy level is expected according to the Gaussian Orthogonal Ensemble model (GOE) of Dyson [22]. Conversely, if there are approximately good quantum numbers still present, levels with different quantum numbers interact very weakly with each other. The spectrum is then formed by the superposition of several non-interacting GOE sequences (one per quantum number) and when a large number of sequencies are present, the distribution of the energy levels becomes indistinguishable from a random (Poisson) distribution.

The degree of spectral rigidity has been tested on the Q and R branches of both the observed first order states. The results obtained (see fig. 4.4 and 4.5) point to a random (Poisson) distribution of the energy levels in all four cases, which implies that the spectum does not consist of a single GOE sequence, but rather of several non-interacting ones, corresponding to approximately good quantum numbers that are conserved on the time-scale explored by the experiment.

Before proceding further, one word of caution must be issued. As already pointed out before, one must be careful about a possible bias of the test produced

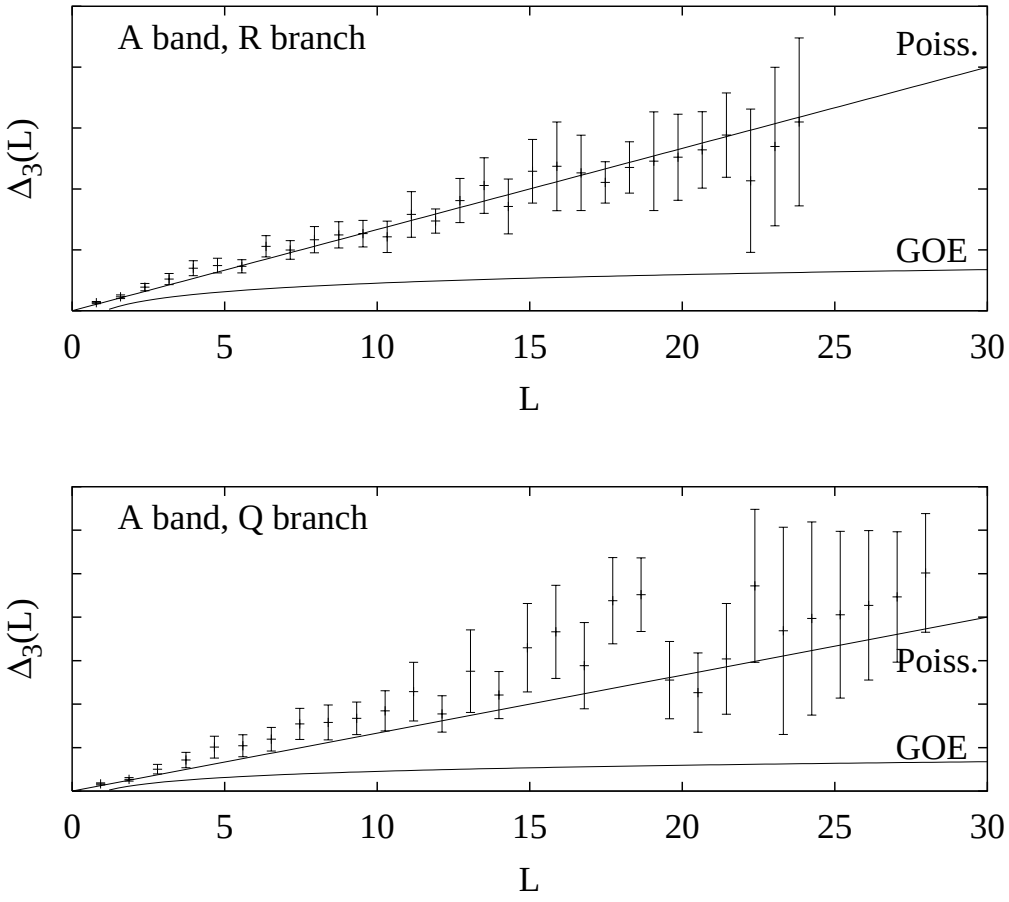

Figure 4.4: Δ_3 statistics for the "A" band of benzene CH overtone at 6005.5 cm^{-1}. L is normalized to the average level spacing. The limiting cases $\Delta_3(L) = L/15$ and $\Delta_3(L) = (\ln L - 0.0687)/\pi^2$, respectively, for a Poisson and GOE level distribution are also plotted for comparison

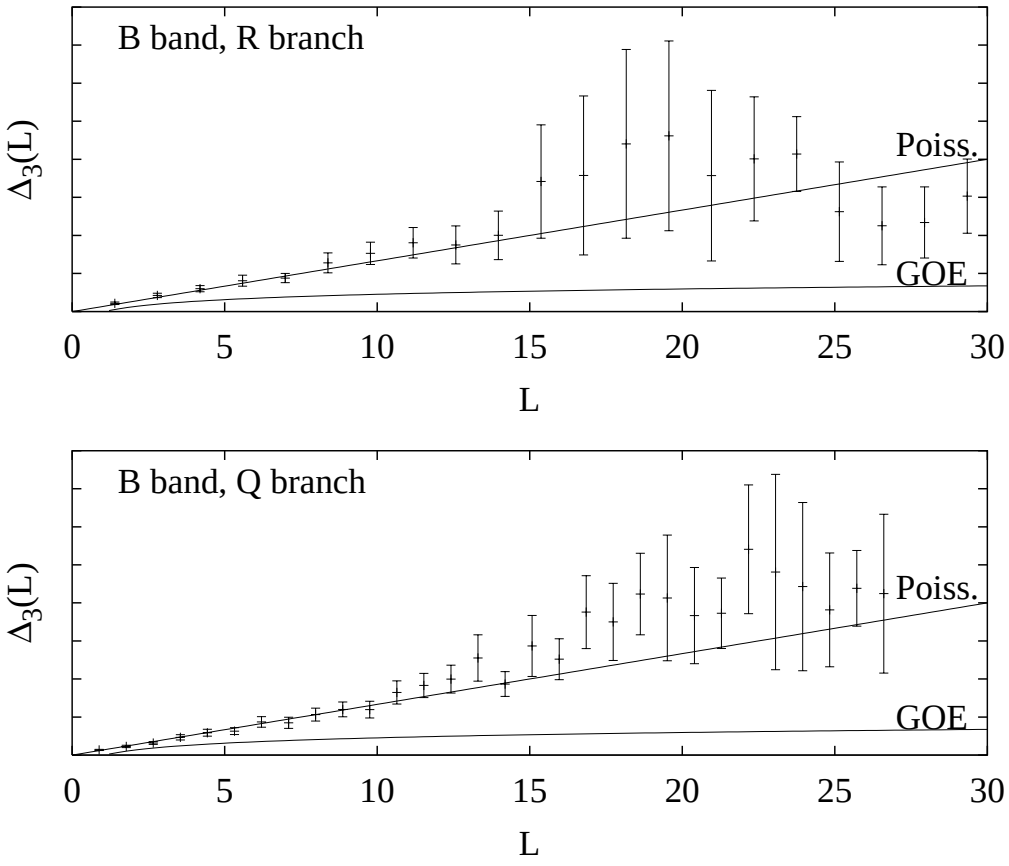

Figure 4.5: Δ_3 statistics for the "B" band of benzene CH overtone at 5999.3 cm^{-1}. L is normalized to the average level spacing. The limiting cases $\Delta_3(L) = L/15$ and $\Delta_3(L) = (\ln L - 0.0687)/\pi^2$, respectively, for a Poisson and GOE level distribution are also plotted for comparison

	A band		B band	
	$J = 2$	$J = 3$	$J = 2$	$J = 3$
f	< 0.07	< 0.05	< 0.15	< 0.07
ρ_{app}	68 ± 8	59 ± 7	85 ± 10	105 ± 10
ρ	> 970	> 1180	> 560	> 1500

Table 4.3: Parameters corresponding to the maximum of the likelihood function of eq. 4.3 for the observed spectra of benzene. The uncertainties given are one standard deviation.

by incomplete sequences produced by the finite signal-to-noise ratio. In order to rule out this possibility we have performed the following test: we have assumed that the spectrum actually *does* consist of a single GOE sequence of unknown density ρ, and only a fraction f of the levels are observed, and then checked whether the assumption is consistent with the observed spacings. Lehmann and Coy [23] give a formula for the expected level spacing distribution $P(s)$ as a function of f and $\rho_{\mathrm{app}} = f\rho$ (the apparent density of states), which is used here to calculate the likelihood function:

$$\mathcal{L}(\rho_{\mathrm{app}}, f) = \prod_i P(s_i, \rho_{\mathrm{app}}, f) \tag{4.3}$$

for the set of observed spacings $\{s_i\}$. As prescribed by standard statistical methods [24] the best estimate for f and ρ_{app} is given by the values that maximize the likelihood function. The results obtained are reported in tab. 4.3. It is obvious that if the hypothesis being tested is true, the real density of bath states must be much higher than the density of vibrational states (ρ_{calc}) calculated before and even of the $(2J + 1)\rho_{\mathrm{calc}}$ expected in the unlikely case of complete breakdown of the K symmetry produced by Coriolis coupling. There is therefore strong evidence that the hypothesis of a single sequence is not compatible with the observed spectra and must be rejected.

Determining the exact number of sequences present in the spectrum is not possible, given the small number of states observed, but an estimate can be found based on the reasonable assumption that at least 50% of the states are actually observed and on the following, simple consideration. For a spectrum composed of several arbitrary sequences, each with fractional density ρ_i [25]:

$$\Delta_3(L) = \sum \Delta_3(\rho_i L) \tag{4.4}$$

Missing 50% of the levels gives the same contribution to the fluctuation of the number of levels in the interval L as a sequence with fractional density $1/2$, (i.e. $1/2\ L/15$). Since in all cases the observed Δ_3 does not deviate from the $L/15$ line up to $L = 25$, the remaining contribution must come from the presence of several GOE sequences. The number of sequences required to explain the observed data is 6 in the case where they all have the same fractional density, higher in all other cases. We can therefore safely conclude that under the above assumptions, the presence of at least 6 independent sequences is required to explain the observed data. This conclusion implies the presence of 6 conserved quantum numbers, whose nature and identity are at present unknown to us. In particular it is not clear yet whether the sequences correspond to different values of the same quantum number or to different quantum numbers altogether. In general, it's not surprising to observe that the dynamics still exhibit some remnants of order. Indeed this has been previously observed for other molecules, such as NO_2, at a time-scale on the order of 200 ps [26]. What is surprising in our case is that this happens for such a—comparatively speaking—big molecule as benzene, even on the very long time scale (25 ns) explored by the experiment.

4.4 Summary and Conclusions

An analysis of the eigenstate resolved spectrum of benzene in the region of the first C-H stretching overtone and comparison with previously reported results reveals a highly non-ergodic energy redistribution dynamics, involving several different time-scales. The dynamics produces a highly mixed, but not statistical—even at infinite time—distribution of vibrational excitation. In light of these results the assumptions made by RRKM and other statistical approaches for the calculation of chemical reaction rates in large polyatomic molecules should perhaps be reconsidered.

Bibliography

[1] K. V. Reddy, Donald F. Heller, and Michael J. Berry. Highly vibrationally excited benzene: Overtone spectroscopy and intramolecular dynamics of C_6H_6, C_6D_6, and partially deuterated or substituted benzenes. *J. Chem. Phys.*, 76(6):2814–2837, March 1982.

[2] Edwin L. Sibert III, William P. Reinhardt, and James T. Hynes. Intramolecular vibrational relaxation and spectra of CH and CD overtones in benzene and perdeuterobenzene. *J. Chem. Phys.*, 81(3):1115–1134, 1984.

[3] Mario Scotoni, Andrea Boschetti, Nadia Oberhofer, and Davide Bassi. The $3 \longleftarrow 0$ CH stretch overtone of benzene: An optothermal study. *J. Chem. Phys.*, 94(2):971–977, January 1991.

[4] R. H. Page, Y. R. Shen, and Y. T. Lee. Infrared-ultraviolet double resonance studies of benzene molecules in a supersonic beam. *J. Chem. Phys.*, 88:4621–4636, 1988.

[5] R. H. Page, Y. R. Shen, and Y. T. Lee. Local modes of benzene and benzene dimer, studied by infrared-ultraviolet double resonance studies of benzene molecules in a supersonic beam. *J. Chem. Phys.*, 88:5362–5376, 1988.

[6] Christophe Iung and Robert E. Wyatt. Time-dependent quantum mechanical study of intramolecular vibrational energy redistribution in benzene. *J. Chem. Phys.*, 99(3):2261–2264, August 1993.

[7] Yongfeng Zhang and R. A. Marcus. Intramolecular dynamics III. Theoretical studies of the CH overtone spectra for benzene. *J. Chem. Phys.*, 97(8):5283–5295, 1992.

[8] F. Iachello and S. Oss. Vibrational modes of polyatomic molecules in the vibron model. *J. Mol. Spectr.*, 153:225–239, 1992.

[9] A. Callegari, H. K. Srivastava, U. Merker, K. K. Lehmann, G. Scoles, and M. Davis. Eigenstate resolved infrared-infrared double-resonance study of intramolecular vibrational relaxation in benzene: first overtone of the CH stretch. *J. Chem. Phys*, 106:432–435, 1997.

[10] Lauri Halonen. Local mode vibrations in benzene. *Chem. Phys. Lett.*, 87(3):221–225, March 1982.

[11] M. L. Junttila, J. L. Domenech, G. T. Fraser, and A. S. Pine. Molecular-beam optothermal spectroscopy of the $9.6 - \mu$m ν_{14} band of benzene. *J. Mol. Spectr.*, 147:513–520, 1991.

[12] G. Herzberg. *Molecular spectra and molecular structure*, volume II. Infrared and raman spectra of polyatomic molecules. Van Nostrand, New York, 1945.

[13] J. Pliva and A. S. Pine. Analysis of the 3-μm bands of benzene. *J. Mol. Spectr.*, 126:82–98, 1987.

[14] Daniele Romanini and Kevin K. Lehmann. Numerical Laplace transform density of states calculation, for medium and large molecules, in

the harmonic and first-order anharmonic approximations. *J. Chem. Phys.*, 98:6437–6444, 1993.

[15] L. Goodman, A. G. Ozkabak, and S. N. Thakur. A benchmark vibrational potential susface: ground-state benzene. *J. Phys. Chem.*, 95:9044–9058, 1991.

[16] B.H. Pate, K.K. Lehmann, and G. Scoles. *J. Chem. Phys.*, 95:3891, 1991.

[17] M. Quack. On the density and number of rovibronic states of a given symmetry species: rigid and nonrigid molecules, transition states and scattering channels. *J. Chem. Phys.*, 82:3277–3283, 1985.

[18] J. A. Nicholson and W. D. Lawrance. Evidence that irreversible intramolecular vibrational energy redistribution is slow for ring modes up to 8200 cm^{-1} in S_0 benzene. *Chem. Phys. Lett.*, 236:336–342, 1995.

[19] Martin Gruebele and Robert Bigwood. Molecular vibration energy flow: beyond the golden rule. *Int. Rev. Phys. Chem*, Submitted.

[20] Martin Gruebele. Intramolecular vibrational dephasing obeys a power law at intermediate times. *Proc. Natl. Acad. Sci. USA*, Submitted.

[21] S. Schofield and P. G. Wolynes. *J. Chem. Phys.*, 98:1123–1131, 1993.

[22] Freeman J. Dyson. Statistical theory of energy levels of complex systems I. *J. Math. Phys.*, 3(1):140, Jan-Feb 1962.

[23] K. K. Lehmann and S. L. Coy. The gaussian orthogonal ensemble with missing and spurious levels: a model for experimantal level-spacing distributions. *J. Chem. Phys.*, 87:5415–5418, 1987.

[24] P. E. Bevington and D. K. Robinson. *Data reduction and error analysis for the physical sciences*. McGraw-Hill, 1992.

[25] M. Robnik. Recent developments in energy level statistics in generic systems between integrability and chaos. *Progress Theor. Phys.*, Supplement No. 116:331–345, 1994.

[26] K. K. Lehmann and S. L. Coy. The optical spectrum of NO_2: Is it or isn't it chaotic? *Ber. Bunsenges. Phys. Chem.*, 92:306–311, 1988.

Chapter 5

The CH stretch overtone spectrum of pyrrole

5.1 Introduction

Of the three aromatic molecules presented in this study, pyrrole (C_4H_5N), shown in fig 5.1, is the one with the lowest symmetry: C_{2v}. The structure and vibrational spectrum of pyrrole have been investigated several times since the first reported data and vibrational analysis of Lord and Miller [1] experimentally by microwave [2–4] and Infrared/Raman [5–8] spectroscopy, as well as theoretically with *ab initio* [9] and algebraic methods [10]. The CH stretch fundamentals have been investigated in the past at low resolution by various authors [11–13] with sometimes contradictory assignments. Held and Herman [7] have carried out a high resolution investigation of the fundamental CH region which has resolved the ambiguity of the previous assignments. The same experiment didn't give quite as satisfactory results in the overtone region which remains at present to be understood.

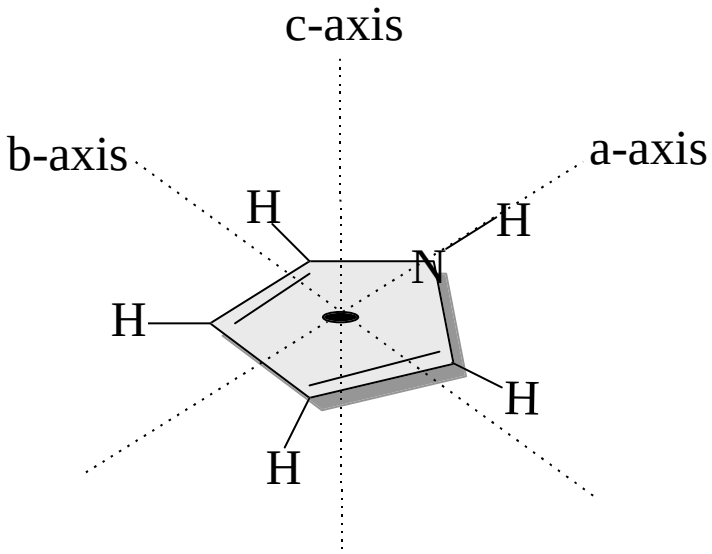

Figure 5.1: Structure and principal axes of pyrrole

On the theoretical side, Lubich and Oss [10] have addressed the overtone problem starting from a semi-empirical one-dimensional algebraic model based on which they predict the position and intensity of all the overtones and combination bands of the CH and NH stretches in the 6000-7000 cm^{-1}region.

While the above mentioned studies have given a reasonably clear picture of the structure and vibrational spectrum of pyrrole, only a few of them have paid some attention to its vibrational dynamics [6–8, 10] (all on a timescale shorter than 1 ps). To the best of our knowledge, the vibrational dynamics of pyrrole at longer times has never been investigated before in either the fundamental or the overtone region.

5.2 Theoretical issues

The low degree of symmetry of pyrrole has important consequences both on its spectroscopy and its dynamics. From a purely spectroscopical point of view the absence of a high order (> 2) symmetry axis makes pyrrole an asymmetric top, with all the 24 normal modes of vibration infrared allowed. Microwave studies [2, 3] have shown that the ring bond lengths and angles are equal to within a few percent, which makes the molecule a nearly oblate symmetric top ($\kappa = 0.9438$), most of the asymmetry being caused by the difference in mass between the nitrogen and the carbon atoms in the ring.

From the point of view of dynamics, the reduced symmetry with respect to e.g. benzene implies that the vibrational states are distributed among a smaller number of symmetry classes, so there is a higher probability that two states belong to the same class and therefore interact. On the other hand pyrrole has more classes of inequivalent bonds than benzene, so the vibrations are likely to be more localized and effective couplings less strong. Since both the topology and the strength of the couplings are different, a different dynamics is expected.

Lastly, for symmetric top molecules, the projection K of the angular mo-

mentum on the high symmetry molecular axis is a strictly conserved quantum number. This is true as long as no significant interaction (Coriolis coupling) occurs between vibration and rotations—and only states with the same J and K can interact. On the contrary, asymmetric tops lack a high symmetry axis and K is—at best—an approximately good quantum number, provided the molecule is reasonably close to a symmetric top. In this case, states with the same J but different K are no longer forbidden to interact, which, in principle, increases the density of coupled states by a factor $2J + 1$. In practice, since pyrrole is very nearly a symmetric top the coupling between states with different K is expected to be weak at low J and become significant only at high J.

The increase in the available density of states due to the lower symmetry is offset by the decrease of the total density of states due to the smaller number of atoms—10 vs. 12 for pyrrole and benzene respectively—so the expected density of coupled states is calculated to be 30 % below that of benzene.

5.3 Experimental

The experimental apparatus has been described in detail in chapter 2. In short, a cold molecular beam of pyrrole is formed by co-expanding a 1 % mixture of pyrrole in helium through a 50 μm nozzle in a vacuum chamber. Upon collimation by a 0.5 mm skimmer, the beam enters a second vacuum chamber where it is probed by an infrared 1.5 μm laser and detected further downstream by means of a cryogenically cooled silicon bolometer. The laser excitation occurs inside a resonant power build-up cavity placed across the beam that enhances the effective laser power experienced by the beam by a factor of 500 in this wavelength region.

For this specific experiment a few changes have been made to the spectrometer and the experimental procedure, as described below. Instead of preparing

a pre-mixed sample of pyrrole in helium, the mixture was formed directly at the gas inlet of the spectrometer by bubbling pure helium through a stainless steel cylinder containing liquid pyrrole (Acros, 99 % purity). This has the advantage that the dilution of the mixture can be easily changed by changing the temperature of the cylinder, which is useful for molecules, like pyrrole, that have a strong tendency to form dimers in the expansion. Dimer formation is prevented also by keeping the nozzle and the gas inlet line heated to about 70 °C, which also prevents pyrrole from condensing inside the gas inlet line.

The laser power coupled to the build-up cavity has been reduced with neutral density filters to about 15 mW when recording the final version of the spectrum since at full power (90 mW) most of the strongest transitions in the spectra appeared noticeably saturated.

For the purpose of labelling the different rotational states, we have added to the spectrometer the capability of doing microwave-infrared double resonance. Microwave radiation from a Hewlett Packard 8350B frequency sweep oscillator fitted with a Hewlett Packard 83595A RF plug-in can be coupled into the spectrometer through a mica window and brought to the interaction region by a 30 cm long strand of (P band) flexible waveguide. About 20 dBm of microwave radiation tunable from 0.01 to 26.5 GHz is available at the output of the plug-in. The exact frequency of the microwave radiation is constantly monitored with an oven-stabilized frequency counter with a precision of $1/10^8$. The rotational transitions used to label the spectrum are reported in tab. 5.1. In all cases the microwave frequency was tuned to the strongest hyperfine component.

Since the available power is more than sufficient to saturate the strong rotational transitions of pyrrole, we have made no attempt to optimize the efficiency of the coupling out of the flexible waveguide, nor to get a well collimated microwave beam in the region of interaction with the molecular beam. A ≈ 2 mm gap in the waveguide allows for the insertion of a metal chopper blade in the

$J''_{K''_a,K''_c} \rightarrow J'_{K'_a,K'_c}$	$F'' \rightarrow F'$	Frequency (MHz)	Rel. Intensity
$3_{1,3} \rightarrow 3_{1,2}$	$2 \rightarrow 2$	22657.85	0.212
	$3 \rightarrow 3$	22656.35	0.280
	$4 \rightarrow 4$	22657.48	0.402
$3_{0,3} \rightarrow 3_{2,2}$	$2 \rightarrow 2$	22671.71	0.212
	$3 \rightarrow 3$	22670.18	0.280
	$4 \rightarrow 4$	22671.29	0.402

Table 5.1: Rotational transitions of pyrrole in the frequency range covered by the microwave synthesizer. The most intense hyperfine components ($F'' \rightarrow F' = 4 \rightarrow 4$) have been used for the double resonance assignment of the spectrum

microwave path which we use to modulate the microwave power seen by the molecular beam. When the double resonance scheme is in use, the microwave is chopped, otherwise the infrared laser is. In both cases the chopping frequency is set around 280 Hz, the exact value depending on where the voltage noise across the bolometer is minimum at time of the experiment. The bolometer signal is synchronously detected with a lock-in amplifier (Stanford Research 510) and recorded as the laser frequency is continuously scanned across the region of interest. In the case of single resonance spectra, all transitions are detected and they appear in the spectrum as positive peaks whose height is proportional to the population of the lower state and the fraction of bright state character carried by the upper state. In the case of a double resonance experiment instead, only those infrared transitions whose ground state population is affected by the microwave are detected. They appear as both positive or negative peaks depending on whether the shared state is the upper or lower state of the microwave transition. The double resonance signal is reduced with respect to the

single resonance signal by a factor which is inversely proportional to the amount of rotational populations displaced by the microwaves. At the rotational temperature of the beam ($\approx$ 6 K), the difference in population of the lower and upper state of a typical ($\approx$ 20 GHz) microwave transition is only about 15 %. This number is further reduced by slightly more than a factor of 2 because only one hyperfine component of the microwave transition can be pumped at a given time. In order to get maximum signal to noise, all the available laser power was coupled to the build-up cavity, even if this produced saturation of the strong lines, since reliable values for the intensities could be obtained from the single resonance spectrum. In spite of this, weak lines that are clearly observable in the single resonance spectrum disappear into the noise when double resonance is used (see fig. 5.3).

Also, most of the transitions observed in the single resonance spectrum do not share a state with a convenient microwave transition, so double resonance was used only for a partial assignment of the spectrum, which was then completed with the standard technique of ground state combination differences on the single resonance spectrum.

5.4 Results and Discussion

Figure 5.2 shows the observed (upper) and simulated (lower) stick spectra of pyrrole CH stretching first overtone around 6145 cm^{-1}. The band has been assigned by Lubich and Oss [10] to the a-type $2\nu_{14}$ overtone. Despite the extensive fractionation (about 3000 lines are observed), the rotational structure typical of the perpendicular band of a planar symmetric top—clusters of lines separated by a distance $2(A-B)$—is clearly recognizable. This already puts a visual upper limit to the IVR rate since the width of each multiplet must be smaller than the spacing ($\approx$ 0.3 cm^{-1}) between the clumps. The pseudo Q-branch occurring

in the a-type spectra of near oblate molecules [14, 15] is not prominent in the molecular beam spectrum. This band—originating from the superposition of many $J_{K_a,K_c} = J_{0,J} \rightarrow J_{0,J-1}$ and $J_{K_a,K_c} = J_{0,J-1} \rightarrow J_{0,J}$ transitions—is very prominent in low resolution spectra taken at room temperature (where high-J states are populated and the transitions are not individually resolved), but is not significant at the high resolution and low temperature typical of molecular beam spectra.

The simulation was performed with a modified version [16] of the fortran program Asyrot [17] with the parameters of table 5.2 and spin statistics 10, 10, 6, 6 for *ee*, *eo*, *oo* and *oe* species respectively.

	Ground state		Upper state	
Param.	Value	Ref.	Value	Ref.
T	6 K		6 K	
ν_0	-		6145.7 cm^{-1}	
A	0.30456 cm^{-1}	[4]	3.022 cm^{-1}	[10]
B	0.30025 cm^{-1}	[4]	3.011 cm^{-1}	[10]
C	0.15117 cm^{-1}	[4]	1.590 cm^{-1}	[10]

Table 5.2: Parameters used for the simulation of the molecular beam spectrum of pyrrole

With the help of the simulated spectrum, spectral assignment has been carried out looking for combination differences involving transitions to the same J_{K_a,K_c} state: since the ground state of the infrared transition is not fractionated, any fractionation pattern of a ro-vibrational transition must be due exclusively to IVR in the upper state and, therefore, it must be the same for all transitions to the same final state even if they originate from different ground rotational states. When—as in this case—the ground state rotational constant are known

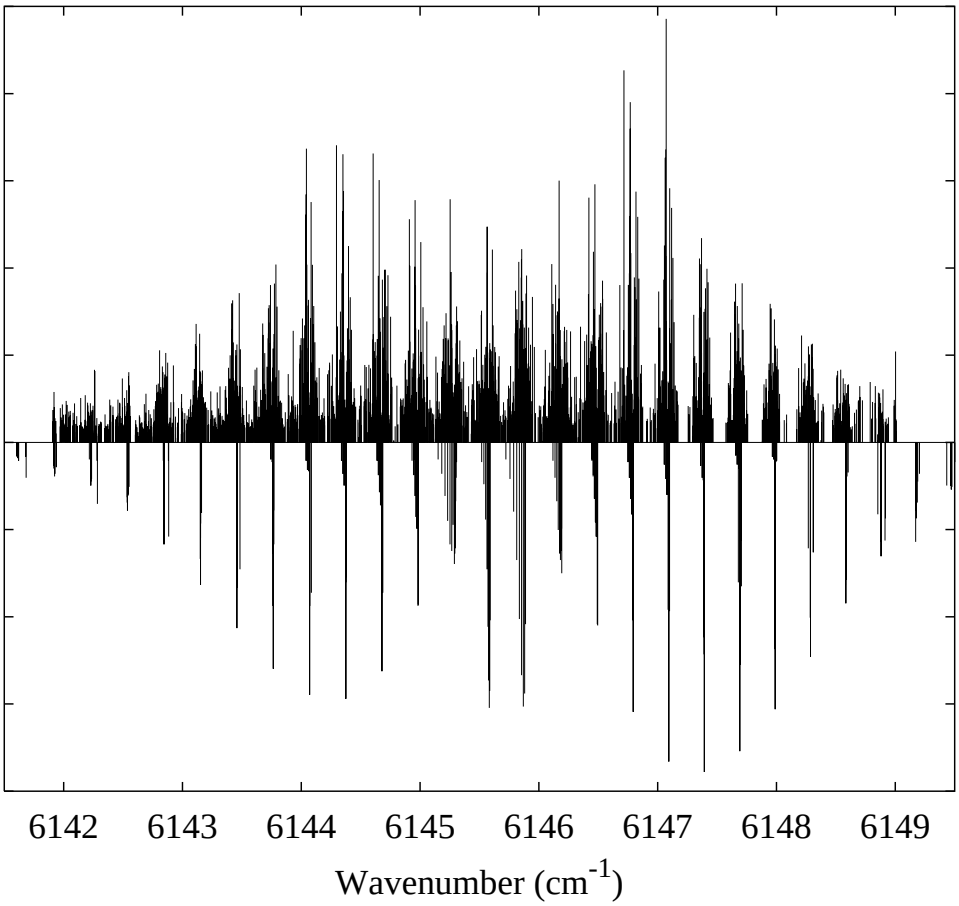

Figure 5.2: Observed (upper) and simulated (lower) molecular beam overtone spectra of pyrrole

with sufficient accuracy, assignment of the spectrum is possible by looking for identical patterns of lines (corresponding to transitions to the same final state) separated by the same energy difference as the ground rotational levels. A large fraction of the about 3000 lines observed in the spectrum have been assigned in this way, and among them the strong progression $J_{0,J} \rightarrow (J+1)_{0,J\pm1}$, which will be extensively discussed since it gives a good insight into the J dependence of IVR.

The assignments have been confirmed by using a microwave-infrared double resonance technique to assign some of the multiplets (see fig. 5.3)

Comparison between the structure of IVR multiplets that correspond to different final states (fig. 5.4) shows—as it was observed for benzene—that the splitting pattern remains roughly constant as J changes, which is an indication of the fact that anharmonic coupling dominates over Coriolis coupling in determining the general features of the vibrational dynamics. In all cases the transition is split into a multiplet of 20 to 30 lines spread over an interval of 0.15 to 0.25 cm^{-1}.

For the purpose of a quantitative discussion, all the relevant statistical properties of the rotational states assigned are collected in table 5.3. The measured density of coupled states (ρ) ranges between 92 and 251 per cm^{-1}, and is, in all but two cases, higher than the density of purely vibrational states ($\rho_{\mathrm{vib}} = 93/cm^{-1}$) calculated with the Laplace transform method described in chapter 3. The measured values increase almost monotonically with J, which indicates breakdown of the K symmetry by Coriolis coupling. Conversely the average coupling strength between the bright state and the dark states decreases with J, which is contrary to the quadratic increase with J which would be expected if the onset of Coriolis coupling between bright and bath states were the dominant effect associated with the increase in J. Clearly the situation is more complex and deserves further discussion which will be focused on the $J_{0,J}$ pro-

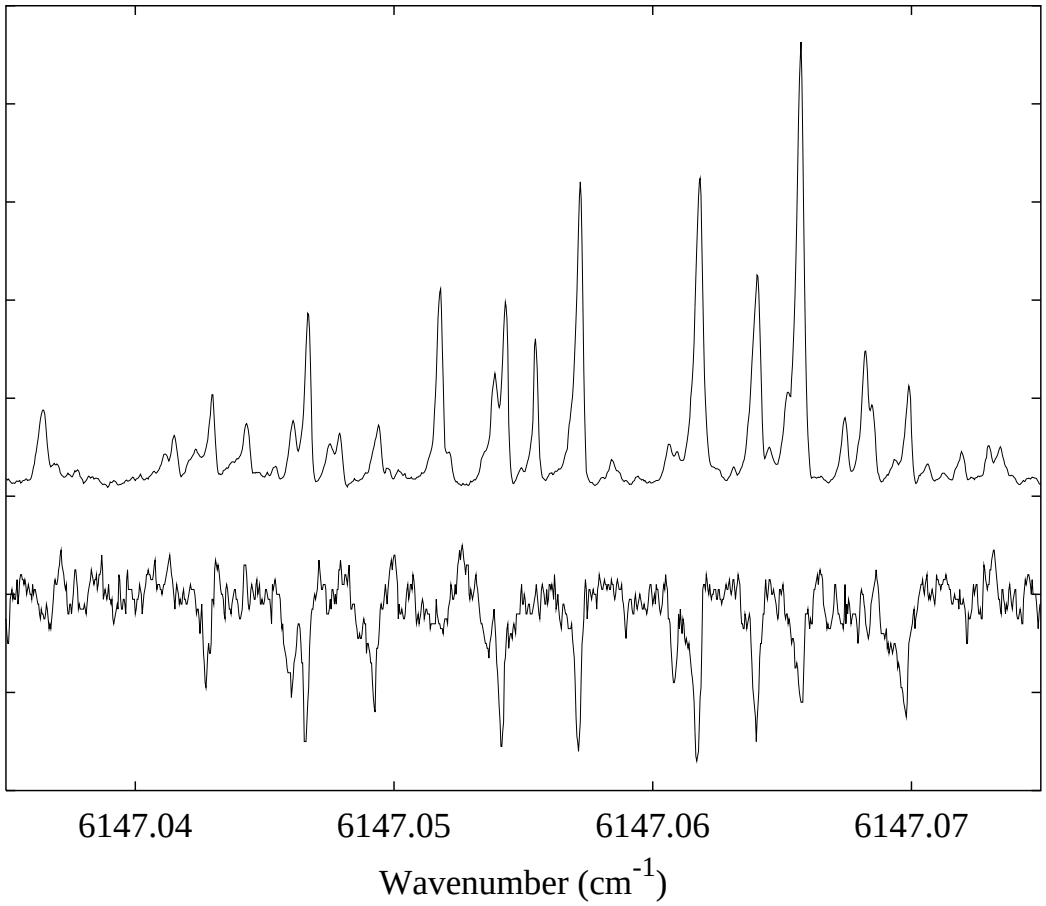

Figure 5.3: A portion of the IR single resonance (top) and IR-MW double resonance (bottom) spectra of pyrrole

$J'_{K'_a,K'_c} \leftarrow J''_{K''_a,K''_c}$	N_d	$\langle V_{\rm rms}\rangle$	$\sum V_i^2$	ρ	$\tau_{\rm GR}$	$N_{\rm eff}$
		(10^{-2}) cm^{-1}	$(10^{-2}$cm$^{-1})^2$	1/cm^{-1}	ps	
$2_{02} \leftarrow 1_{01}$	20	1.24	30.7	92	60	15.1
$2_{02} \leftarrow 3_{03}$	20	1.21	29.2	92	63	12.4
$3_{03} \leftarrow 2_{02}$	21	0.926	18.0	112	88	15.7
$3_{03} \leftarrow 2_{02}$	21	0.892	16.7	112	95	12.6
$4_{04} \leftarrow 3_{03}$	32	0.682	14.9	166	109	17.6
$4_{04} \leftarrow 5_{05}$	32	0.725	16.8	166	98	18.2
$5_{05} \leftarrow 4_{04}$	23	0.712	11.6	154	108	16.6
$5_{05} \leftarrow 6_{06}$	23	0.715	11.7	154	107	18.0
$6_{06} \leftarrow 5_{05}$	19	0.595	6.7	243	98	15.4
$6_{06} \leftarrow 7_{07}$	19	0.606	6.9	243	95	13.7
$7_{07} \leftarrow 6_{06}$	23	0.595	8.1	251	95	19.9
$7_{07} \leftarrow 8_{08}$	23	0.603	8.3	251	92	19.2
$8_{08} \leftarrow 7_{07}$	18	0.615	6.8	216	103	15.7
$8_{08} \leftarrow 9_{09}$	18	0.647	7.5	216	93	15.8

Continues on next page

Continued from previous page

$J'_{K'_a,K'_c} \leftarrow J''_{K''_a,K''_c}$	N_d	$\langle V_{\rm rms}\rangle$	$\sum V_i^2$	ρ	$\tau_{\rm GR}$	$N_{\rm eff}$
		(10^{-2}) cm^{-1}	$(10^{-2}\text{cm}^{-1})^2$	1/cm^{-1}	ps	
$2_{21} \leftarrow 2_{20}$	27	0.934	23.5	147	66	18.6
$2_{21} \leftarrow 3_{22}$	27	0.901	21.9	147	71	15.1
$3_{12} \leftarrow 2_{11}$	22	0.808	14.3	110	117	13.1
$3_{12} \leftarrow 2_{11}$	22	0.722	11.4	110	147	14.4
$3_{21} \leftarrow 3_{22}$	22	0.736	11.9			
$4_{23} \leftarrow 3_{22}$	25	0.584	8.5	145	170	
$4_{23} \leftarrow 5_{24}$	25	0.698	12.1	145	119	

Table 5.3: Statistical properties of pyrrole spectrum for different upper rotational states: average ($\langle V\rangle$) and total coupling ($\sum V_i$) to the bath, number (N_d) and density ρ of observed coupled states, lifetime from Fermi's golden rule ($\tau_{\rm GR}$). The effective number of coupled states ($N_{\rm eff}$), calculated from the normalized spectral intensities ($\{I_i\}$) as $1/\sum I_i^2 - 1$, is also reported for later comparison with triazine.

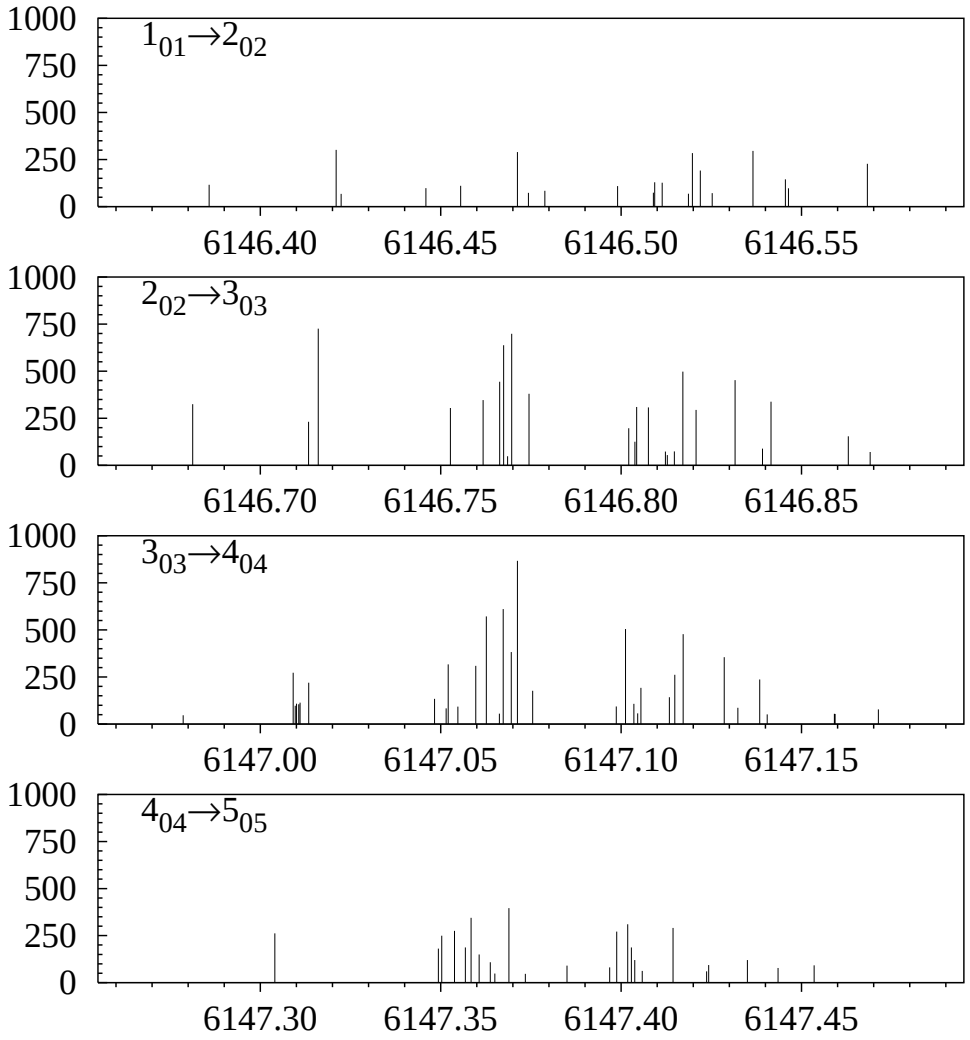

Continues on next page.

gression (shown in fig. 5.4), which is the strongest and most complete among those observed.

Some changes are visible in the progression, not only in the number of coupled states, but especially in the intensity distribution of the multiplets, which, at low J, tend to be spread more evenly and on a wider range than at higher J. Although the disappearance of some of the weak lines in the wings of the mul-

Continuing from previous page

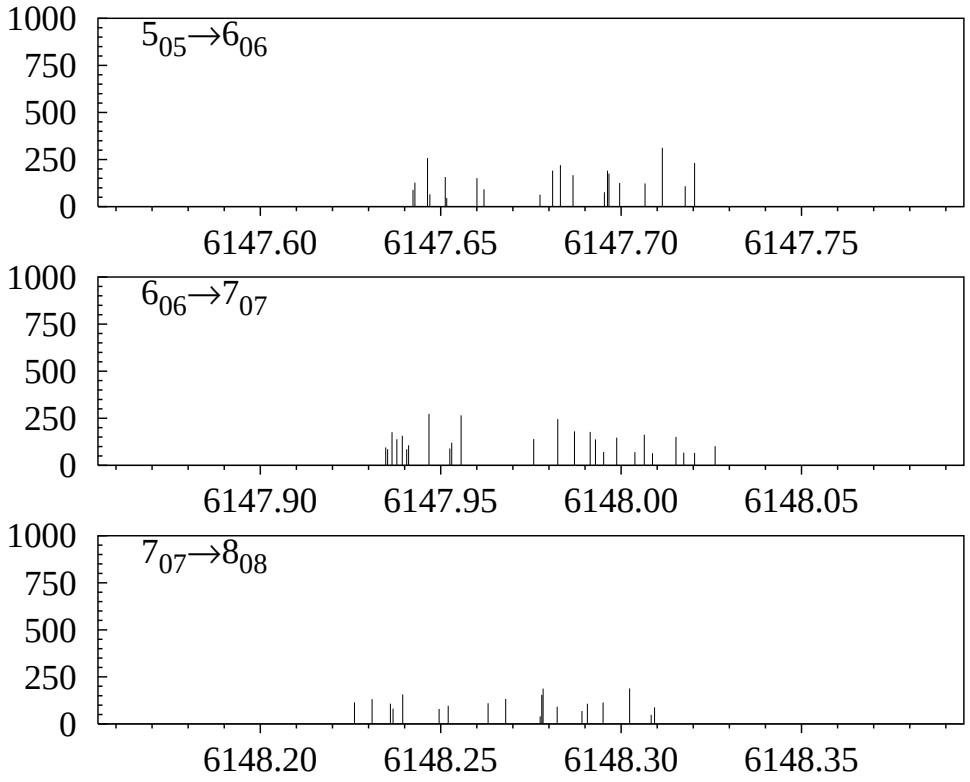

Figure 5.4: Stick spectra of the J_{0J} progression of the $2\nu_{14}$ CH overtone of pyrrole

tiplet could be simply attributed to the lower signal-to-noise ratio of the higher J transitions, a comparison between the $1_{01} \rightarrow 2_{02}$ and $5_{05} \rightarrow 6_{06}$ multiplets which are observed with approximately the same signal-to-noise ratio, shows remarkable differences in terms of density of states and distribution of intensities. The 2_{02} state has a rather sparse structure with an average density of states of $92/\mathrm{cm}^{-1}$(in good agreement with the calculated $93/\mathrm{cm}^{-1}$), while for the 6_{06} state, the density rises to $243/\mathrm{cm}^{-1}$, which is too high to be classified as due to a purely vibrational bath and requires instead that K breakdown is taken into account. Furthermore, the intensity of the observed transitions is distributed over a 0.25 cm^{-1} energy range in the 2_{02} case but only over a 0.15 cm^{-1} in the 6_{06} case. The same trend is clearly visible in the whole J_{0J} progression, even as one accounts for possible effects originating from differences in the signal to noise ratio. A similar behavior has been observed by Pate [18, 19] in the rotational transitions from highly mixed vibrationally excited states of propargyl alcohol and was in that case attributed to the averaging of the rotational constants by IVR in a way analogous to the well known phenomenon of motional narrowing in NMR spectroscopy. In our case the same mechanism can be used to explain the narrowing of the multiplet under the following assumptions:

- the bright state is directly coupled by anharmonic coupling to a primary bath of dark states formed by all the vibrational states with the same J and K as the bright state, with density ρ_{vib} ($\approx 90/\mathrm{cm}^{-1}$).

- The dark states in turn are coupled by Coriolis coupling to a secondary, denser bath formed by all the vibrational states originating from the breakdown of the K symmetry. In principle the density of this bath can be as high as $((2J+1)\rho_{\mathrm{vib}}/\mathrm{cm}^{-1})$ if all the different K states are coupled although, as a first approximation, Coriolis coupling directly connects only states that differ in K at most by 1 [20].

The narrowing corresponds, in this case, to the highly mixed secondary bath

coupling to the primary bath states, thereby averaging their properties, and in particular their "bright state" character. We can think pictorially of the initial excitation of the bright state randomly "hopping" on the lattice formed by the coupled vibrational states. When the lattice density increases, but the hopping probability stays constant, the average distance traveled in a given time, corresponding to the width of the multiplet, decreases. The above hypothesis is supported also by the similarity between different J_{0J} multiplets, as far as the coarse structure is concerned. In particular, while the intensities of specific eigenstates change dramatically with J and states appear and disappear, their positions don't change significantly, which implies that the "skeleton" of the multiplet is determined by anharmonic coupling, while the fine details depends on the increased number of states available at high J and the coupling to them.

In order to test the Coriolis hypothesis, we have performed a simple test constructing a synthetic hamiltonian with the primary bath-secondary bath structure mentioned above. As a primary bath we have taken the dark states resulting from the Lawrance-Knight deconvolution of the $1_{0,1} \rightarrow 2_{0,2}$ multiplet, along with their couplings to the bright state. As a secondary bath we have taken a dense bath of states ($500/\mathrm{cm}^{-1}$) coupled with each other by random gaussian matrix elements with variance $W_{d'd'} = 0.01$ cm^{-1}. The coupling between the primary and secondary bath is also gaussian, with a different variance ($W_{dd'}$) that can be varied to simulate the onset of Coriolis coupling. The corresponding matrix is diagonalized and a new spectrum is found. The results of the simulation are shown in fig. 5.5 for values of $W_{dd'} = 0$, 0.001, 0.002, 0.005, 0.01. Although the results are not expected to reproduce in detail the observed spectra (fig. 5.4) narrowing of the multiplet and redistribution of the spectral intensities is clearly visible as $W_{dd'}$ increases.

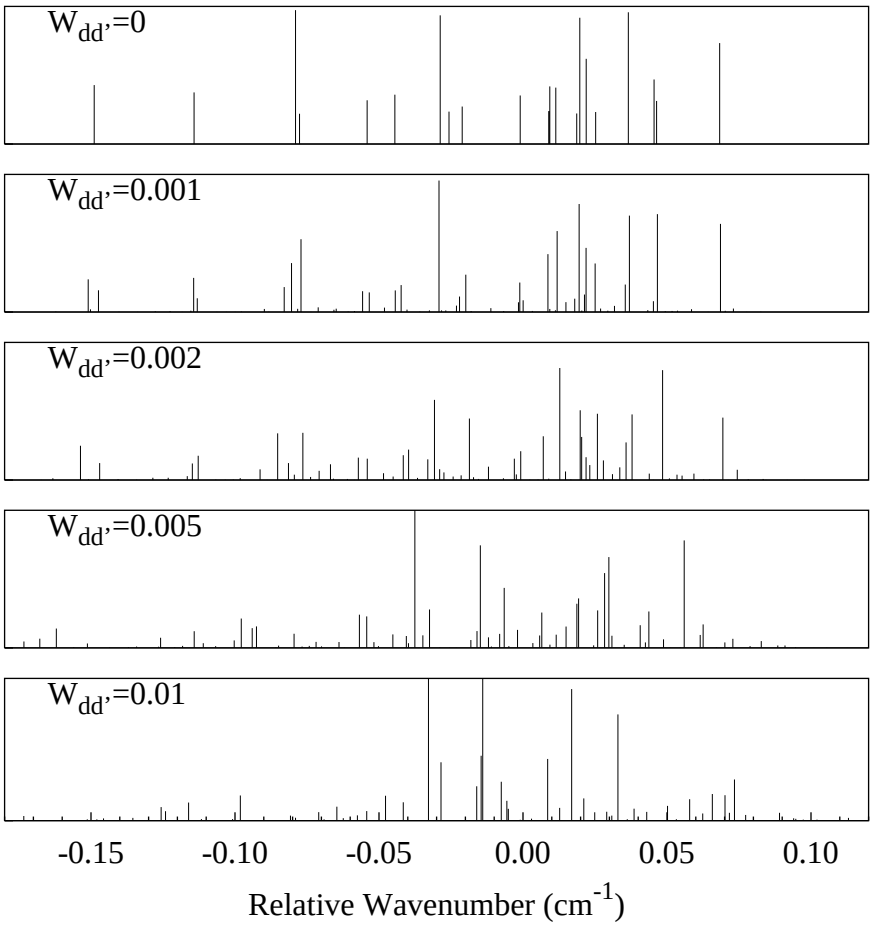

Figure 5.5: Simulation of the intensity distributon pattern of a multiplet as a function of the strength of Coriolis coupling between the dark states. The top panel is the observed $2_{0,2}$ state. In the lower panels the increased average coupling $W_{dd'}$ of the spectrum with the bath of Coriolis states (0.001, 0.002, 0.005 and 0.01 cm^{-1} going from top to bottom) produces a visible narrowing of the multiplet.

J_{K_a,K_c}	f	ρ_{app}	ρ
2_{02}	< 0.1	90 ± 20	> 900
3_{03}	< 0.16	130 ± 20	> 812
4_{04}	< 0.18	180 ± 30	> 1000
5_{05}	0.3 ± 0.2	165 ± 30	> 550
6_{06}	< 0.3	240 ± 50	> 720
7_{07}	0.3 ± 0.15	267 ± 40	> 590
8_{08}	< 0.4	210 ± 50	> 525

Table 5.4: Parameters corresponding to the maximum of the likelihood function of eq. 4.3 for the observed spectra. The uncertainties given are one standard deviation

5.4.1 Level spacing statistics

The presence of sub-structure in the IVR multiplets raises—as in the case of benzene discussed in section 4.3.1—the question of whether there could be any approximately good quantum numbers that are preserved on the timescale investigated. The small number of coupled states observed does not allow the same testing of the long range order (Δ_3) that was carried on in the case of benzene, therefore only the level spacing distribution will be analyzed here. On the other hand, the observed onset of Coriolis coupling offers the possibility of "tuning" the strength of coupling between the bath states and studying the dependence of the dynamics on the degree of mixing of the bath.

As in the case of benzene, we make the hypothesis that the observed multiplets originate from a single GOE sequence of unknown density (ρ), of which only a fraction f is observed, and test if the hypothesis is compatible with the observed data. The results of the test are listed in table 5.4.

For the low J states ($J \leq 4$) the value of ρ necessary to explain the observed

spacing distribution with a single GOE sequence is higher than the calculated density of states, even considering the $(2J+1)\rho_{\mathrm{calc}}$ expected in the case of complete breakdown of the K symmetry produced by Coriolis coupling. As in the case of benzene, the hypothesis must therefore be rejected in favor of the presence of two or more non interacting sequences. For the higher J states, instead, mixing of the bath states due to the stronger Coriolis coupling produces a more GOE-like behavior, but the data available do not allow to determine whether or not the full GOE limit is reached.

5.5 Conclusions

As already observed for benzene, the eigenstate resolved spectrum of pyrrole shows that the low J states exhibits remnants of order in their fractionation pattern and eigenstate distribution, corresponding to non-ergodic IVR dynamics. This residual order is—in part or totally—destroyed by Coriolis coupling of the bath for the higher J states.

Taking the low J states as representative of the rotationless dynamics of pyrrole, for later comparison with the other molecules investigated, a lower limit of 60 ps can be put on the lifetime of the excited vibration, with most states averaging around 90 ps (see table 5.3). In comparison with the values observed for benzene, the lifetime is at least 3 to 4 times longer, despite the fact that the nature of the vibration excited is the same and the density of states available for coupling is similar. This is probably due to the higher symmetry of benzene's normal modes which makes them more likely to share the motion of common atoms which, in turn, increases the probability of large low order couplings between them.

Bibliography

[1] R. C. Lord and F. A. Miller. *J. Chem. Phys.*, 10:328, 1942.

[2] B. Bak, D. Christensen, L. Hansen, and J. Rastrup-Andersen. *J. Chem. Phys.*, 24:720, 1956.

[3] L. Nyagaard, J. T. Nielsen, J. Kirchheiner, G. Maltesen, J. Rastrup-Andersen, and G. O. Sørensen. Microwave spectra of isotopic pyrroles, molecular structure, dipole moment and ^{14}N quadrupole coupling constants of pyrrole. *J. Mol. Struct.*, 3:491, 1969.

[4] G. Wlodarczak, L. Martinache, J. Demaison, and B. P. Van Eijck. The millimeter-wave spectra of furan, pyrrole, ans pyridine: experimental and theoretical determination of the quartic centrifugal distortion constants. *J. Mol. Spectr.*, 127:200–208, 1988.

[5] T. D. Klots, R. D. Chirico, and W. V. Steele. Complete vapor phase assignment for the fundamental vibrations of furan, pyrrole and tiophene. *Spectrochimica Acta*, 50 A:765–795, 1994.

[6] C. Douketis and J. P. Reilly. The NH stretch in pyrrole: a study of the fundamental ($\Delta\nu = 1$) and third overtone ($\Delta\nu = 4$) bands in the bulk gas and in a molecular beam. *J. Chem. Phys.*, 96:3431–3440, 1992.

[7] A. Held and M. Herman. High resolution spectroscopic study of the first overtone of the N-H stretch and of the fundamentals of the C-H stretches in pyrrole. *Chem. Phys.*, 190:407–417, 1995.

[8] A. Mellouki, R. Georges, M. Herman, D. L. Snavely, and S. Leytner. Spectroscopic investigation of the ground state pyrrole ($^{12}C_4H_5N$): the N-H stretch. *Chem. Phys.*, 220:311–322, 1997.

[9] Y. Xie, K. Fan, and J. E. Boggs. The harmonic force field and vibrational spectra of pyrrole. *Mol. Phys.*, 58:401–411, 1986.

[10] L. Lubich and S. Oss. Vibrational spectroscopy of CH/NH stretches in pyrrole: an algebraic approach. *J. Chem. Phys*, 106:5379–5392, 1997.

[11] R. Cataliotti and G. Palliani. *Can. J. Chem*, 54:1473, 1976.

[12] R. Navarro and J. M. Orza. *An. Quim.*, 79:557, 1982.

[13] M. G. Sowa, B. R. Henry, and Y. Mizugai. *J. Chim. Phys.*, 95:7659, 1991.

[14] J. M. Brown. *J. Mol. Spectr*, 31:118, 1969.

[15] K. K. Innes and J. E. Parkin. *J. Mol. Spectr.*, 21:66, 1966.

[16] C. Zauli. An extended version of asyrot. *Computer Phys. Comm.*, 79:555, 1994.

[17] F. W. Birss and D. A. Ramsay. Computer assistance in the analysis of molecular spectra. *Computer Phys. Comm.*, 38:83, 1984.

[18] B. A. Pate. The rotational spectrum of a highly vibrationally mixed quantum state I. Intramolecular vibrational energy redistribution (IVR) exchange narrowing of the rotational spectrum. *J. Chem. Phys.*, Submitted.

[19] B. A. Pate. The rotational spectrum of a highly vibrationally mixed quantum state II. The eigenstate resolved analog to dynamic nuclear magnetic resonance (NMR) spectroscopy. *J. Chem. Phys.*, Submitted.

[20] J. E. Wollrab. *Rotational spectra and molecular structure*. Academic Press, New York, 1967.

Chapter 6

The CH Stretch Overtone Spectrum of 1,3,5-Triazine

6.1 Introduction

1,3,5-Triazine, $C_3N_3H_3$ (henceforth referred to simply as triazine or *s*-triazine) was chosen as the last term in this comparative study because of its intermediate characteristics between benzene and pyrrole. In analogy with benzene, the delocalized character of the normal modes arising from the high molecular symmetry (D_{3h}) is expected to enhance the average couplings. On the other side the presence of inequivalent atoms in the ring is expected to have a depressing effect on the couplings since different modes are less likely to share the motion of a common atom, in analogy to—and possibly to a larger extent than—what is observed in pyrrole. How the IVR dynamics is affected by these contrasting effects and whether one of them dominates over the other is the subject of the investigation described in this chapter.

Being the most symmetric of its three possible isomers and the most stable

one, *s*-triazine is also the most studied and best characterized. Its molecular structure and vibrational modes and those of some of its derivatives have been determined experimentally by infrared/raman spectroscopy [1–5], electron [1, 5] and neutron [6] scattering and theoretically by *ab initio* calculations [1, 3, 5–7]. Triazine dynamics has been the subject of a number of investigations [8–11], mostly in the excited electronic surface, in the attempt to determine the exact nature of the photodissociation mechanism (two step vs. concerted triple dissociation) which recently lead to the finding of experimental evidence [8] in favor of the two step mechanism. The IVR lifetime of the ν_6, $2\nu_6$ and $\nu_6 + \nu_{12}$ vibrational modes (Lord's numbering [12]) in the S_1 electronic surface, whith excess energy 670, 1170 and 1750 cm^{-1} has been determined by fluorescence spectra [9,10] to be 310, 280 and 260 ps respectively. The interpretation of these data is unfortunately complicated by the interaction with the nearby triplet state vibrational manifold. On the other hand very little is known about the dynamics of the molecule in the ground electronic state potential energy surface.

6.2 Experimental

Given the slow scan rate of the spectrometer ($\approx 1 cm^{-1}$ /hr), a precise knowledge of the the band center position of the vibrational transition under investigation can save several hours of explorative scanning. Since no information on the C-H overtone region was available from previous studies, a survey gas cell FTIR spectrum has been collected with the departmental Nicolet 700 spectrometer. The triazine beam was made by expanding a 0.5 % mixture of triazine in helium, prepared by flowing 400 kPa helium gas through a stainless steel cilinder containing a few grams of solid triazine (Aldrich 97% purity, used without further purification). Air was eliminated from the container by repeated cycles of pumping and flushing with helium. The container was refilled every four hours

with fresh triazine in order to ensure a reasonably constant beam composition.

Both the container and the gas line connecting it to the nozzle were kept at a temperature of about 75 °C, in order to increase the triazine concentration, while the nozzle was kept at a higher temperature (≈ 90°C) in order to avoid condensation and its possible clogging. The remaining parameters of the experimental setup were left as described for the previous two molecules.

6.3 Results and Discussion

The fundamental vibrational modes of triazine [1] are listed in table 6.1, along with their symmetry and Infrared/Raman activity. Five bands are expected to carry significant infrared intensity in the first CH stretching overtone region. They all have E' symmetry since the only other infrared active species (A'' symmetry) all involve out of plane antisymmetric vibrational modes that don't have in plane CH stretching character which gives absorption intensity in this spectral region. The five bands derive from various combinations of the E' symmetry Fermi dyad ν_6 (CH stretching) $2\nu_7^2$ (ring breathing mode overtone) with the A' symmetry levels ν_1 (symm. CH stretching) and $2\nu_7^0$, namely: $\nu_1+\nu_6$, $2\nu_6^2$, $\nu_1 + 2\nu_7^2$, $\nu_6 + 2\nu_7^0$ and $\nu_6 + 2\nu_7^2$. A low resolution FTIR spectrum of the overtone region (fig. 6.1) shows the most intense band (centered around 5980 cm^{-1}) which was chosen for our investigation. Based on its frequency and its Coriolis constant (ζ) (obtained from the molecular beam spectrum) the band has been tentatively assigned to the $\nu_6 + 2\nu_7^2$ combination. The labeling is clearly only approximate since all the states are likely to be mixed with each other since they all have the same symmetry.

The eigenstate resolved spectrum of the region between 5978 and 5985 cm^{-1}—as observed in the molecular beam—is reported in the upper panel of fig 6.2. In the same figure the spectrum simulated with a symmetric top hamiltonian

Mode	Freq. (cm^{-1})	Symmetry	Activity
ν_1	3052.1	A'_1	R
ν_2	1138.1	A'_1	R
ν_3	989.7	A'_1	R
ν_4	1375	A'_2	R
ν_5	1000	A'_2	R
ν_6	3062.91	E'	IR/R
ν_7	1556.34	E'	IR/R
ν_8	1409.96	E'	IR/R
ν_9	1172.64	E'	IR/R
ν_{10}	675.68	E'	IR/R
ν_{11}	926.59	A''_2	IR
ν_{12}	736.74	A''_2	IR
ν_{13}	1032	E''	IR/R
ν_{14}	339.50	E''	IR/R

Table 6.1: Frequency, symmetry and activity of the fundamental modes of 1,3,5-Triazine, from ref. [1]

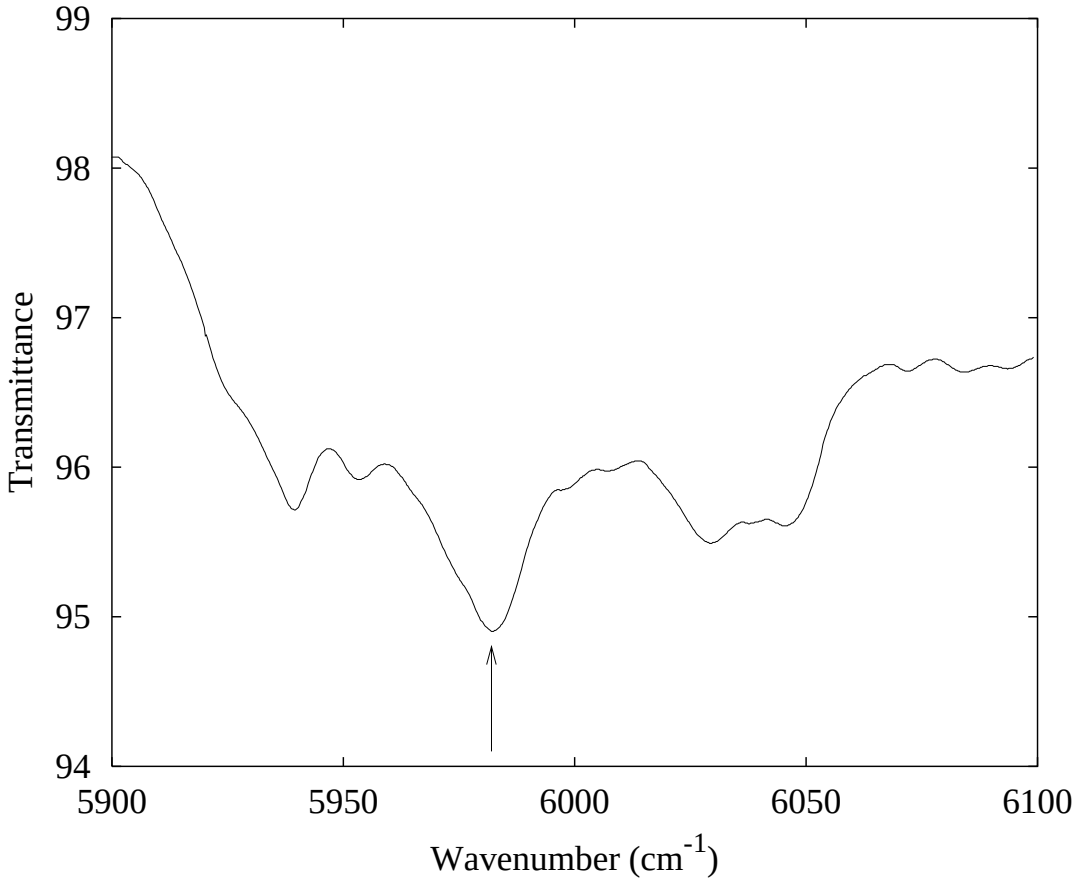

Figure 6.1: Low resolution Fourier transform spectrum of triazine in the CH stretching overtone region. The band studied here is indicated by an arrow.

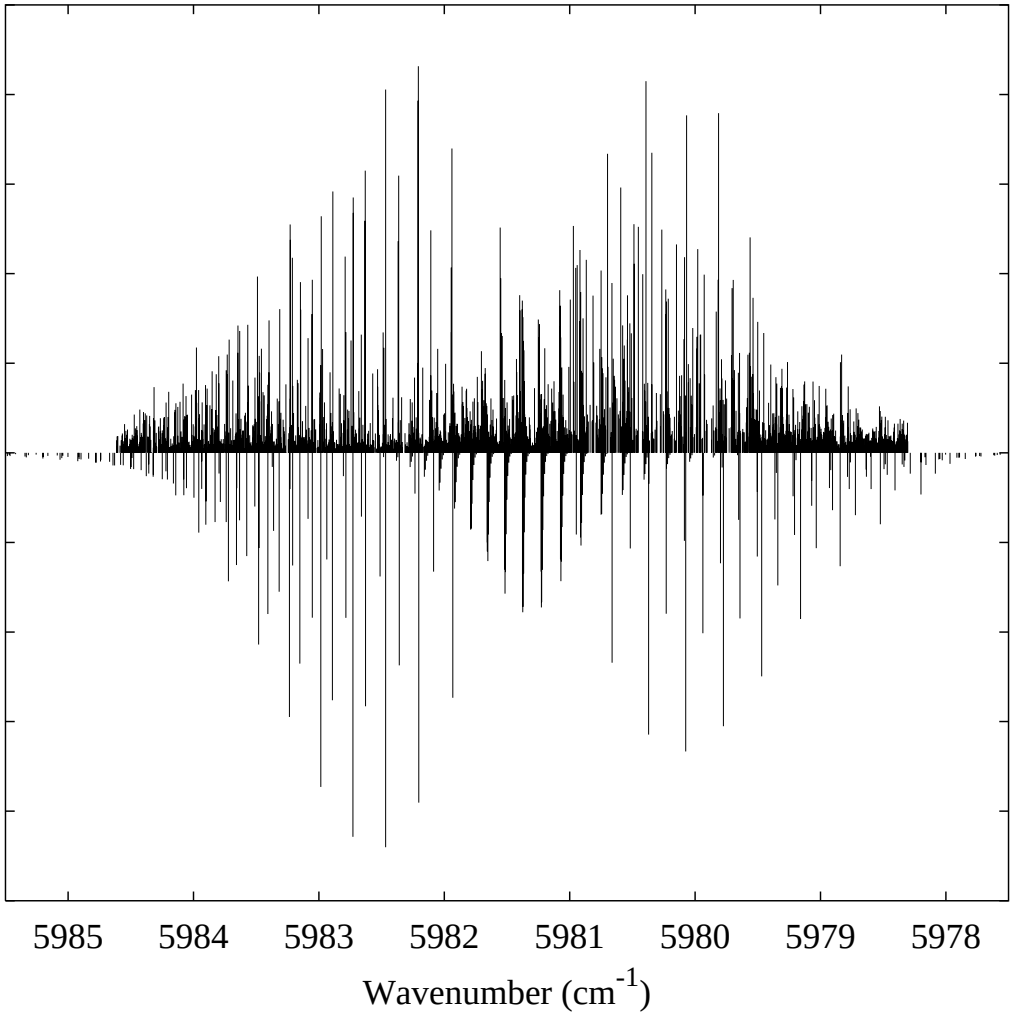

Figure 6.2: Observed (upper) and simulated (lower) molecular beam overtone spectra of triazine

(eq. 6.1) and the parameters of table 6.2 is also shown (lower panel).

The experimental spectrum is evidently more congested since its transitions undergo IVR fragmentation. Despite the fractionation the perpendicular band structure expected for a CH stretching band in a planar molecule is recognizable

Molecular constants				
	Lower State		Upper State	
Param.	Value	ref.	Value	ref.
T (K)	4		4	
ν_0 (cm^{-1})	-		5981.27	fit
B (cm^{-1})	0.21486156(10)	[1]	0.21419(5)	fit
C (cm^{-1})	0.1074	[1]	0.10481(3)	fit
D (cm^{-1})	$5.3433(58) \times 10^{-8}$	[1]	same	
ζ	-		-0.3246(9)	fit

Spin weights [4]			
$K = 0$, J even	$K = 0$, J odd	$K = 3p \pm 1$	$K = 3p$
70	70	146	140

Table 6.2: Parameters used for the simulation of the molecular beam spectrum of triazine

indicating a width of the IVR multiplets smaller than the average separation of the rotational lines (≈ 0.2 cm^{-1}).

Since the molecule doesn't have a permanent dipole moment, microwave double resonance techniques cannot be used for assignment of the spectrum, which was carried out using the standard technique of combination differences using the the ground states rotational constants of ref. [4]. To help the assignment a numerical simulation of the spectrum was carried out using a symmetric

top model [13]:

$$\begin{aligned}\nu &= \nu_0 + (B' + B'')m + (B' - B'' - D' + D'')m^2 \\ &\quad -2(D' + D'')m^3 - (D' - D'')m^4 \\ &\quad +[C'(1-2\zeta) - B'] + 2[C'(1-\zeta) - B']k \\ &\quad +[(C' - B') - (C'' - B'')]k^2 \end{aligned} \tag{6.1}$$

where $m = J'' + 1$ for the R branch and $m = -J''$ for the P branch and $k = K''$ for $\Delta K = +1$ transitions and $k = -K''$ for $\Delta K = -1$ transitions. As a first approximation, the upper state rotational constants were set equal to the ground state value and then refined as the assignment progressed.

Of the about 3000 transitions observed in the experimental spectrum, approximately 300 among the most intense have been assigned by combination differences their J and K quantum numbers. Most of the low J, K multiplets are rather complete, so an analysis of the dynamics and its dependence on molecular rotations can be carried out. All the measured parameters relevant to the discussion have been collected in table 6.3.

Let's focus initially on the $J = 0, K = 0$ state, which classically corresponds to the molecule being in a non rotating state. Selection rules [14] forbid Coriolis coupling to this state, so any observed splitting must come from anharmonic coupling. Since only one transition to this state is allowed ($^pP_1(1)$), there is no possiblity of using combination differences for the assignment. Fortunately, as shown in fig. 6.3, $^pP_1(1)$ is well enough isolated in the spectrum: the only overlapping lines belong to the $^qQ_3$ branch which has been reliably assigned, so the remaining lines observed in this portion of the spectrum can be safely assigned to $^pP_1(1)$.

The observed density of states ($90/\text{cm}^{-1}$) is in reasonable agreement with the value of $63/\text{cm}^{-1}$ calculated with the harmonic frequencies of table 6.1 with the Laplace transform technique [15], especially considering that when—as in this

		$J=0$	$J=1$	$J=2$	$J=3$	$J=4$
$K=2\rightarrow 1$	τ	-	-	43	125 ± 5	<600
	ρ	-	-	41	60	210
	N_{eff}	-	-	1.4	1.2	0.8
	N_d	-	-	5	4	2
$K=1\rightarrow 0$	τ	115	115 ± 5	125 ± 10	90 ± 5	145
	ρ	90	60	68	94	142
	N_{eff}	3.5	3.8	3.7	3.7	4.2
	N_d	7	- 6	6	7	10
$K=0\rightarrow 1$	τ	-	90 ± 5	80 ± 5	100 ± 5	
	ρ	-	80	73	40	
	N_{eff}	-	3.2	2.2	1.5	
	N_d	-	5	4	3	
$K=1\rightarrow 2$	τ	-	-	230 ± 20	175	120
	ρ	-	-	65	110	58
	N_{eff}	-	-	1.5	3.1	2.6
	N_d	-	-	4	7	6

Table 6.3: Lifetime (τ, ps), observed density of states (ρ, states/cm^{-1}) and effective number of coupled states (N_{eff}) for different J, K multiplets. The values for the transition $J=0, K=1\rightarrow 0$ are only estimates from a visual assignment, since an assignment based on combination differences is not possible for this transition.

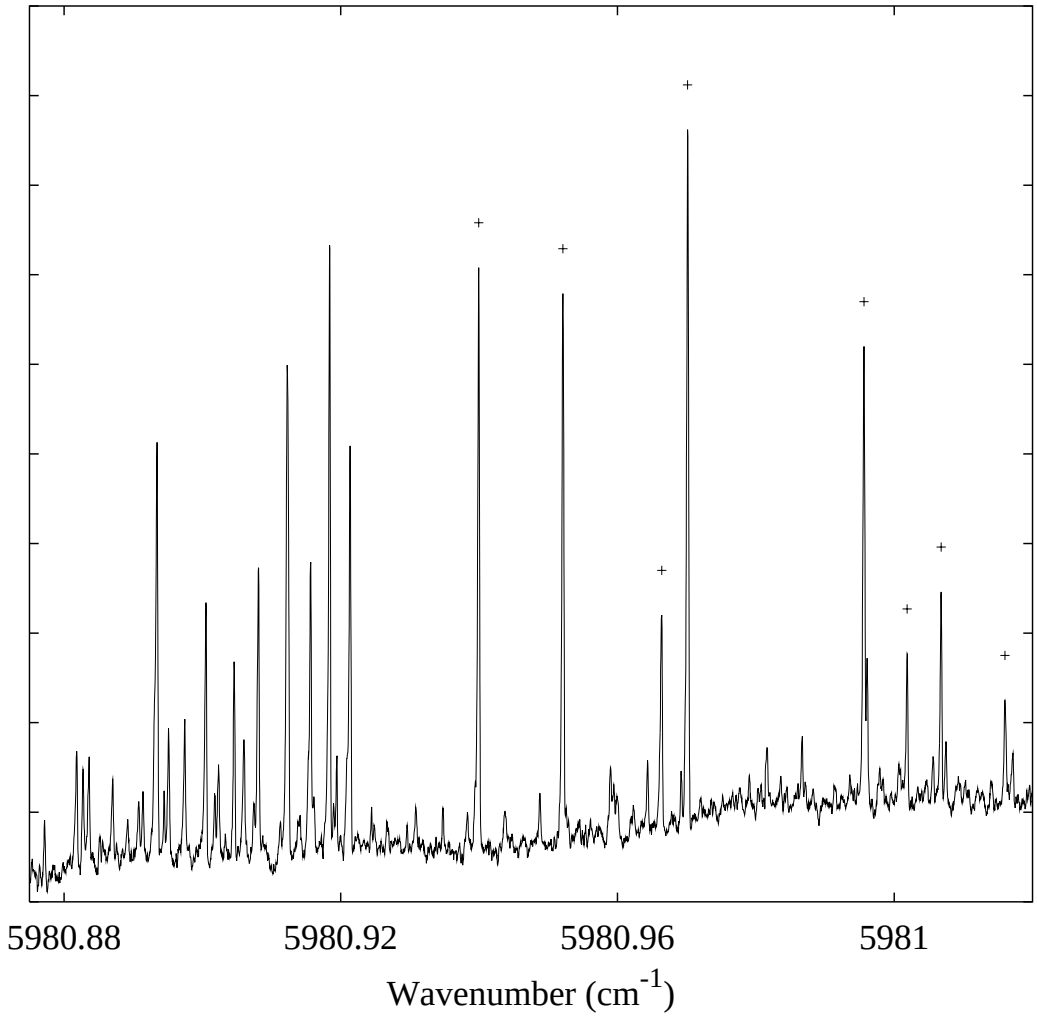

Figure 6.3: Enlarged view of the region near the ${}^{p}P_1(1)$ transition. Lines marked with a cross have been assigned to ${}^{p}P_1(1)$.

case—a small number of coupled states is observed, large statistical fluctuations are possible. Because of the "rotationless" nature of this state, the value of its lifetime is particularly interesting since it gives the rate of IVR as mediated only by vibrational couplings, which is what most theoretical studies deal with. A value of $\tau = 115$ ps can be derived from the measured density of states and the average couplings ($V_{\rm rms} = 8.7 \times 10^{-3}$ cm^{-1}) using the Fermi's golden rule. Comparison with the other J states with $K = 0$ shows a rather constant value of the lifetime at low J with fluctuations at $J - 3, 4$ but no significant trend that would point to an onset of Coriolis coupling.

Inspection of the Fourier transform of the spectrum autocorrelation function (fig. 6.4) shows qualitative agreement with the lifetimes calculated with the Fermi's golden rule, although the non-exponential behavior of the initial decay due to the small number of states present in each multiplet gives consistently longer estimates of the lifetimes. More interestingly, the survival probability exhibits in all cases strong recurrences, indicating incomplete redistribution of the initial vibrational excitation.

Unfortunately, the small number of states observed in each multiplet does not allow the same statistical analysis used in the previous cases to be performed here. Some quantitative comparison can still be made by inspecting the dilution factor f, which is defined as the sum of the square of the normalized spectral intensities:

$$f = \sum I_i^2 \tag{6.2}$$

which measures the "dilution" of the bright state character. Perhaps more immediately evident is the related quantity $N_{\rm eff} = 1/f - 1$ which can be thought of as the number of states effectively coupled to the bright state, since it takes the value of 0 for a multiplet consisting of a single line and $N - 1$ for a multiplet consisting of N equally intense lines.

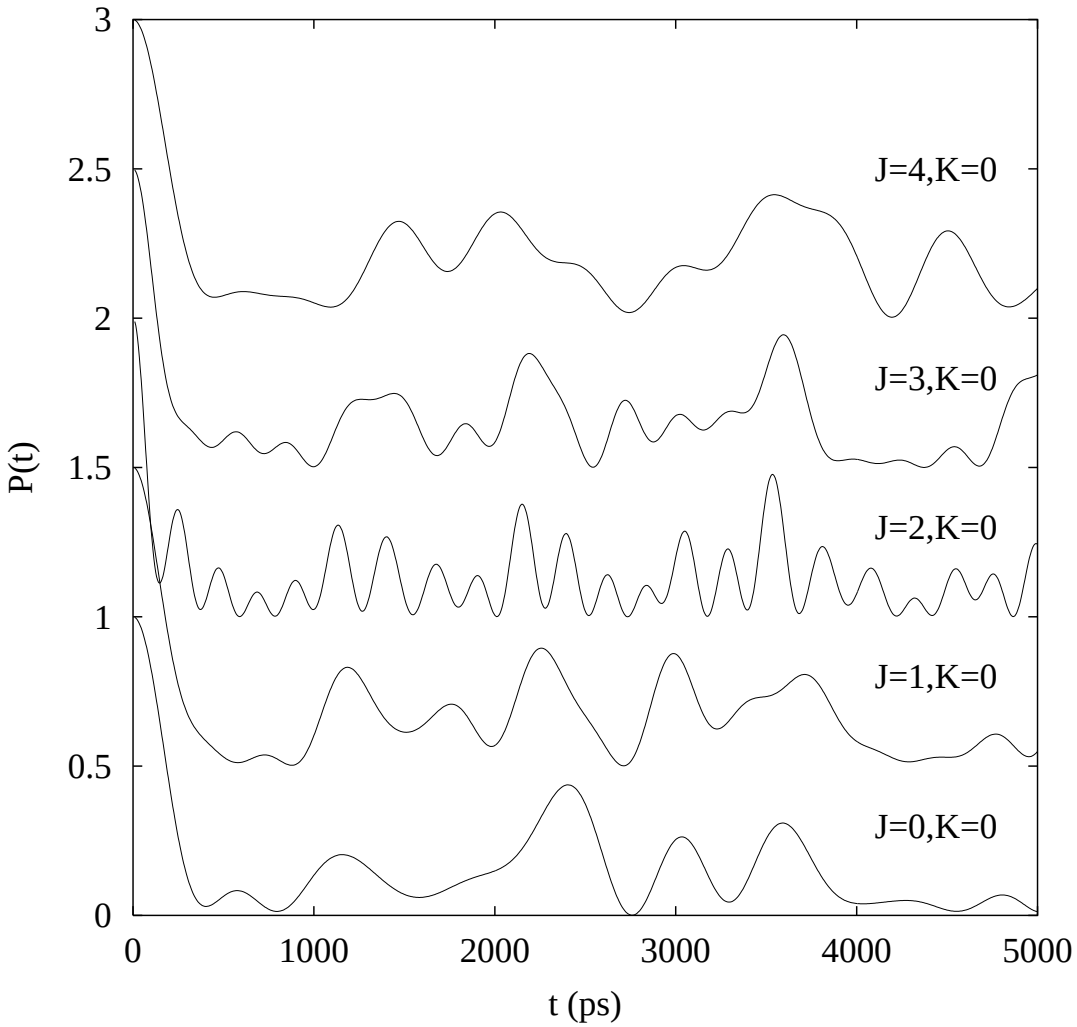

Figure 6.4: Survival probability of the $K = 0$, $J = 0 - 4$ states, calculated from the Fourier transform of the spectrum autocorrelation function. For greater clarity the plots are offset vertically by 0.5 from each other.

The very small numbers reported in table 6.3 for N_{eff} indicate that the coupling of the bright state to the bath is not as extensive as it had been observed for the other molecules in this study. Indeed, while the comparison of the bright state lifetime and coupling to the bath between triazine and pyrrole (115 vs. 60 ps and 8.7 vs 12 $\times 10^{-3}$ cm^{-1} respectively) would induce to think that they have quite similar dynamics, the markedly different number of effectively coupled states shows that this is probably not the case.

6.4 Conclusions

The molecular beam study of triazine carried out in this study shows that, despite having symmetry and structure characteristics intermediate between benzene and pyrrole (the other two molecules studied here), triazine shows in comparison quite a different type of dynamics, characterized by reasonably strong but sparse coupling to the bath. Although a quantitative explanation of these differences will require sofisticated calculations, which are currently underway by Martin Gruebele at the University of Illinois, it can be tentatively speculated that the lack of extensive coupling to the bath is not accidental but rather depends on the different structure of the molecule since the presence of inequivalent atoms in the ring is likely to decouple those vibrational modes that don't share the motion of a common atom.

Bibliography

[1] Carole A. Morrison, Bruce A. Smart, David W. H. Rankin, Heather E. Robertson, M. Pfeffer, W. Bodenmüller, R. Ruber, B. Macht, A. Ruoff, and V. Typke. Molecular structure of 1,3,5-triazine in gas, solution, and crystal phases and by ab initio calculations. *J. Phys. Chem. A*, 101:10029–10038, 1997.

[2] A. Navarro, J. J. Lopez Gonzales, M. Fernandez Gomez, F. Marquez, and J. C. Otero. Vibrational spectra of *s*-triazine and its halogenated derivatives. Harmonic scaled ab initio force field for *s*-triazine, trifluoro-*s*-triazine and trichloro-*s*-triazine.

[3] Gad Fisher, A. U. Nwankwoala, M. P. Ollif, and A. P. Scott. Vibrational spectra of 1,2,3-triazine. *J. Mol. Spectr.*, 161:388–395, 1993.

[4] Wolfram Bodenmüller, Andreas Ruoff, and Laurent Manceron. FTIR study of the ν_{12} and the $\nu_{12} + \nu_{14} - \nu_{14}$ bands of 1,3,5-triazine near 740 cm^{-1}. *Z. Naturforsch.*, 47A:1197–1203, 1992.

[5] W. Pyckhout, I. Callaerts, C. van Alsenoy, and H. J. Geise. The molecular structure of s-triazine in the gas phase determined from electron diffraction, infrared/raman data and by ab initio force field calculations. *J. Mol. Struct.*, 147:321–329, 1986.

[6] A. Navarro, J. J. Lopez Gonzales, G. J. Kearley, J. Tomkinson, S. F. Parker, and D. S. Sivia. Vibrational analysis of the inelastic neutron scattering spectrum of s-triazine and trichloro-s-triazine. *Chem. Phys.*, 200:395–403, 1995.

[7] S. Creuzet and J. Langlet. Theoretical determination of structural parameters for *s*-triazine and some derivatives. comparison between ab initio and semi-empirical calculations. *Chem. Phys. Lett.*, 208:511–516, 1993.

[8] T. Gejo, J. A. Harrison, and J. Robert Huber. Three-body photodissociation of 1,3,5-triazine. *J. Phys. Chem.*, 100:13941–13949, 1996.

[9] N. Ohta and T. Takemura. Rotational dependence of external magnetic field effects on yeld and decay of fluorescence of s-triazine vapor. *J. Chem. Phys.*, 93:877–886, 1990.

[10] N. Ohta and T. Takemura. Magnetic quenching of $S_1 \rightarrow S_0$ sharp fluorescence and broad fluorescence of s-triazine vapor. *J. Phys. Chem.*, 94:3466–3469, 1990.

[11] N. Ohta. Effects on molecular vibration and rotation dynamics in S_1 of s-triazine vapor. *Laser Chem.*, 10:109–138, 1989.

[12] R. C. Lord, A. L. Marston, and F. A. Miller. *Spectrochi. Acta*, 9:113–125, 1957.

[13] G. Herzberg. *Molecular spectra and molecular structure*, volume II. Infrared and raman spectra of polyatomic molecules. Van Nostrand, New York, 1945.

[14] J. E. Wollrab. *Rotational spectra and molecular structure*. Academic Press, New York, 1967.

[15] Daniele Romanini and Kevin K. Lehmann. Numerical Laplace transform density of states calculation, for medium and large molecules, in the harmonic and first-order anharmonic approximations. *J. Chem. Phys.*, 98:6437–6444, 1993.

Chapter 7

Conclusions and final remarks

The results presented in this thesis demonstrates:

1. The very high level of sensitivity and resolution currently achievable in molecular beam spectroscopy of vibrational overtones made possible by modern laser and optical techniques.

2. The usefulness of eigenstate-resolved spectroscopy and double resonance techniques for the detailed study of vibrational energy redistribution mechanisms, even in rather large molecules.

Using the relationship $2\pi\Delta\nu\Delta t \approx 1$, the typical size of the energy range explored (10 cm^{-1}) and the resolution of the spectrometer (2×10^{-4} cm^{-1}) define the boundaries of the time window (500 fs to 25 ns) in which eigenstate resolved spectroscopy is the method of choice for the study of IVR. Furthermore, we have shown that the ability to measure the position of the single eigenstates with high accuracy makes it possible to use statistical methods of analysis to

gain information about the nature of the bath and the strength of the couplings, when direct deperturbation methods are not practicable.

The results of the investigation of the CH stretching overtone of benzene, pyrrole and triazine carried out in this thesis, bear a number of implications in different directions. Despite the fact that properties like the number of atoms, the density of bath states and the nature of the chromophore, are approximately the same in the three cases investigated, still remarkably different dynamics is found, in terms of lifetime, number of effectively coupled states and strength of the couplings. This implies that the above mentioned properties—although certainly important—don't play a dominant role in determining the rate and the extent of the vibrational energy redistribution. The importance of the molecular structure and symmetry and their effects on the couplings between different vibrational modes becomes then apparent.

Benzene and pyrrole also provide a very interesting case for the study of the problem of ergodic vs. non ergodic energy redistribution, which is one of the central problems in the field of IVR. Benzene—having the highest number of coupled states—provides the most compelling answer to the question. Remarkably, in the observed portion of the spectrum there is no evidence of ergodic dynamics, such as spectral rigidity or level repulsion. On the contrary, the hypothesis that the IVR multiplets observed are composed of a single GOE sequence—corresponding to fully ergodic dynamics—must be rejected on the basis of both Δ_3 and level spacing statistical analysis.

Pyrrole, given the smaller number of coupled states, does not give as strong an answer as benzene, but the nice progression of rotational states observed allows for observing the effects of the strength of Coriolis coupling between the bath states. For the low J states no evidence of ergodic dynamics is observed as in the case of benzene, while at higher J the narrowing of the multiplets suggests the possible onset of strong bath mixing.

The variety of behaviors observed for seemingly simple changes of molecular structure and the lack of complications connected with the absence of low frequency, large amplitude modes, should make these molecules challenging but tractable benchmarks for theoretical models of IVR which seek the degree of accuracy needed for a quantitative and predictive theory of IVR in reasonably complex molecules.

At the same time, the non ergodic behavior observed should perhaps induce reconsideration of some of the assumptions of statistical theories for the calculation of chemical reaction rates in large polyatomic molecules.